AD-A055 794 RESEARCH TRIANGLE INST RESEARCH TRIANGLE PARK N C F/G 10/2
PHOTODIODE DESIGN STUDY.(U)
DEC 77 M F LAMORTE F33615-76-C-1283
UNCLASSIFIED AFAL-TR-77-230 NL

1 OF 1
ADA
055794

END
DATE FILMED
8-78
DDC

AFAL-TR-77-230

PHOTODIODE DESIGN STUDY

Research Triangle Institute
Research Triangle Park, North Carolina 27709

DECEMBER 1977

TECHNICAL REPORT AFAL-TR-77-230
FINAL REPORT (SUPPLEMENT) FOR PERIOD MAY-DECEMBER 1977

Approved for public release; distribution unlimited.

AIR FORCE AVIONICS LABORATORY
AIR FORCE WRIGHT AERONAUTICAL LABORATORIES
AIR FORCE SYSTEMS COMMAND (AFSC)
WRIGHT-PATTERSON AIR FORCE BASE, OHIO 45433

NOTICE

When Government drawings, specifications, or other data are used for any purpose other than in connection with a definitely related Government procurement operation, the United States Government thereby incurs no responsibility nor any obligation whatsoever; and the fact that the government may have formulated, furnished, or in any way supplied the said drawings, specifications, or other data, is not to be regarded by implication or otherwise as in any manner licensing the holder or any other person or corporation, or conveying any rights or permission to manufacture, use, or sell any patented invention that may in any way be related thereto.

RUSSELL W. RUNNELS, Project Engineer
Electro-Optic Detectors Group
Electro-Optics Technology Branch

DONALD R. LOCKER, Actg. Chief
Electro-Optic Detectors Group
Electro-Optics Technology Branch

FOR THE COMMANDER

WILLIAM C. SCHOONOVER, Chief
Electro-Optics Technology Branch
Electronic Technology Division

Copies of this report should not be returned unless return is required by security considerations, contractual obligations, or notice on a specific document.

AFSC FORM 0070/17 May 1973 — 75

UNCLASSIFIED

SECURITY CLASSIFICATION OF THIS PAGE (When Data Entered)

REPORT DOCUMENTATION PAGE

READ INSTRUCTIONS BEFORE COMPLETING FORM

1. REPORT NUMBER: AFAL-TR-77-230	2. GOVT ACCESSION NO.
3. RECIPIENT'S CATALOG NUMBER	
4. TITLE (and Subtitle): PHOTODIODE DESIGN STUDY.	5. TYPE OF REPORT & PERIOD COVERED: Final rept. May - Dec 77; Supplemental
6. PERFORMING ORG. REPORT NUMBER	
7. AUTHOR(s): M. F. Lamorte	8. CONTRACT OR GRANT NUMBER(s): F33615-76-C-1283
9. PERFORMING ORGANIZATION NAME AND ADDRESS: Research Triangle Institute, Research Triangle Park, North Carolina 27709	10. PROGRAM ELEMENT, PROJECT, TASK AREA & WORK UNIT NUMBERS: 20010361 03
11. CONTROLLING OFFICE NAME AND ADDRESS: Air Force Avionics Laboratory (DHO), Air Force Systems Command, Wright-Patterson AFB, Ohio 45433	12. REPORT DATE: Dec 77
	13. NUMBER OF PAGES: 78
14. MONITORING AGENCY NAME & ADDRESS (if different from Controlling Office)	15. SECURITY CLASS. (of this report): UNCLASSIFIED
	15a. DECLASSIFICATION/DOWNGRADING SCHEDULE

16. DISTRIBUTION STATEMENT (of this Report)

Approved for public release; distribution unlimited.

62204F

17. DISTRIBUTION STATEMENT (of the abstract entered in Block 20, if different from Report)

18. SUPPLEMENTARY NOTES

19. KEY WORDS (Continue on reverse side if necessary and identify by block number)

Photodiode
Solid State
Electro-Optical

20. ABSTRACT (Continue on reverse side if necessary and identify by block number)

The purpose of this work was to apply the analytical method developed for single junction and multijunction solar cells, Contract No. F33615-76-C-1283, to photodiodes and avalanche photodiodes. It was anticipated that this analytical method will advance the state-of-the-art because of the following: (1) the analysis considers the total photodetector multilayer structure rather than just the depleted region; (2) a model of the complete band

DD FORM 1 JAN 73 1473 EDITION OF 1 NOV 65 IS OBSOLETE

UNCLASSIFIED

SECURITY CLASSIFICATION OF THIS PAGE (When Data Entered)

structure is analyzed; (3) application of the integral form of the continuity equation is used; (4) structures that reduce dark current and/or increase the ratio of photocurrent to dark current are obtained; and (5) structures that increase spectral response in the depleted region and reduce response in other regions of the diode are obtained.

The integral form of the continuity equation developed for solar cells is the steady-state or time-independent form. The contract specified that the time-independent equation would only be employed to determine applicability to photodetectors.

The GaAsSb photodiode under development at Rockwell International, Thousand Oaks, California was used to determine the applicability to photodetectors. The diode structure is composed of four layers grown on a substrate. The analysis in Section 5.0 presents calculations of spectral response. This parameter is used in this study to optimize the structure. Frequency response calculations were not considered.

Section 2.0 briefly discussed the advantages of III-V multilayer photodiode performance over Si avalanche photodiodes and photomultipliers. The development of photodiodes is presented in Section 3.0. Photodiode operating parameters, materials selection and structure are discussed in Section 4.0. Calculations using the steady-state integral form of the continuity equation are presented and dsicussed in Section 5.0.

TABLE OF CONTENTS

FORWARD

This report was prepared by the Center for the Synthesis and Study of Semiconducting Compounds (CSSSC), Research Triangle Institute, Research Triangle Park, North Carolina under Air Force Contract No. F33615-76-C-1283. The contract was administered under the direction of the Air Force Avionics Laboratory, Wright-Patterson Air Force Base, Ohio. Mr. Russell W. Runnels (AFAL/DHO-3) was the Air Force Project Engineer.

The study began in May 1977 and was completed in August 1977. The contributors to this work were M. F. Lamorte and D. Abbott.

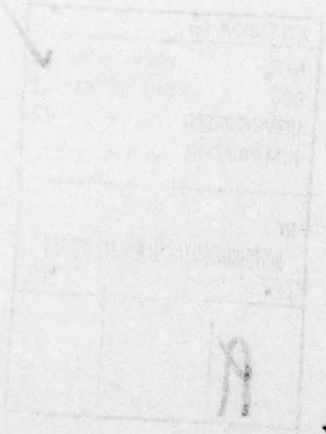

SECTION I

INTRODUCTION

The purpose of this work was to apply the analytical method developed for single junction and multijunction solar cells, Contract No. F33615-76-C-1283, to photodiodes and avalanche photodiodes. It was anticipated that this analytical method will advance the state-of-the-art because of the following: 1) the analysis considers the total photodetector multilayer structure rather than just the depleted region; 2) a model of the complete band structure is analyzed; 3) application of the integral form of the continuity equation is used; 4) structures that reduce dark current and/or increase the ratio of photocurrent to dark current are obtained; and 5) structures that increase spectral response in the depleted region and reduce response in other regions of the diode are obtained.

The integral form of the continuity equation developed for solar cells is the steady-state or time-independent form. The contract specified that the time-independent equation would only be employed to determine applicability to photodetectors.

The GaAsSb photodiode under development at Rockwell International, Thousand Oaks, California was used to determine the applicability to photodetectors. The diode structure is composed of four layers grown on a substrate. The analysis in Section V presents calculations of spectral response. The parameter is used in this study to optimize the structure. Frequency response calculations were not considered.

Section II briefly discusses the advantages of III-V multilayer photdiode performance over Si avalanche photodiodes and photomultipliers. The development of photodiodes is presented in Section III. Photodiode operating

parameters, materials selection and structure are discussed in Section IV. Calculations using the steady-state integral form of the continuity equation are presented and discussed in Section V.

SECTION II

PHOTODETECTORS

Electrooptics technology has become well established in recent years in military and space vehicle applications, and in some instances it is being utilized in industrial applications. Typically at this stage of technological development, methods are being explored to push the technology to its limit using existing hardware. However, it is clear that in some applications the available devices require improved performance to permit the applications to expand. Improved devices may be obtained by fabricating devices from more appropriate material, or more appropriate material combinations, or advanced state-of-the-art device structures.

In data transmission and communication transmission applications where subnanosecond rates and low level signals are encountered, the avalanche photodiode may significantly improve system performance. For many applications Si avalanche photodiodes do not exhibit the performance characteristics required [1]. As a result, III-V materials have been under investigation for photodiodes and avalanche photodiodes.

The ternary GaAsSb has been under intensive investigation for receiver applications at 1.064 μm in PIN structures [2]. However, in GaAsSb PIN photodiodes the avalanche gain, M, must exceed 4 to improve the S/N ratio compared to the performance when M=1, i.e., the photodiode mode of operation which results when the reverse bias is reduced so that the avalanche mode is not present. For $1 < M \leq 2$ the S/N is degraded as photodiode reverse bias is increased because the increase in surface dark current reduces S/N by a factor greater than the increase due to avalanche gain. Increasing M from 2 to 10 increases S/N approximately linearly with M. This results because

S/N is markedly influenced by avalanche gain. In the photodiode (i.e., M=1) at reasonably low leakage currents, the noise is composed of Johnson noise current and preamp equivalent input noise current. The Johnson noise is minimized by choosing as large a loading-resistor as bandwidth requirements permit. This condition represents the limiting performance possible at M=1. The preamplifier noise simply degrades the S/N ratio from the limit set by the Johnson current noise of the load-resistor.

The GaAsSb PIN photodiode without avalanche gain has been compared directly with the ITT S-1 photomultiplier and the General Electric Company Si avalanche photodiode in a 50 Ω preamp receiver [2]. The photomultiplier was selected for 0.1% quantum efficiency at 1.06 μm. The General Electric Company Si avalanche photodiode was a selected device with a quantum efficiency of 30% at 1.06 μm. These data are presented in Table 1. It should be emphasized that both the photomultiplier and the Si avalanche photodiode for the data reported in Table 1 were operated with internal gain while the GaAsSb photodiode was not.

Notwithstanding, the GaAsSb receiver exhibits better performance characteristics than either the Si APD or the S-1 photomultiplier. The Noise Equivalent Power (NEP) with and without incident energy on the detectors shows, under typical operating conditions, that the photomultiplier exhibits 34 times more noise than the GaAsSb receiver, and the Si APD, 3.3 times.

The GE Si APD reported in Table 1 obtains its moderate quantum efficiency by virtue of its extremely wide depletion region. The wide

TABLE 1

NEP COMPARISON BETWEEN S-1 PHOTOMULTIPLIER, Si AVALANCHE PHOTODIODE PREAMPLIFIER RECEIVER AND A GaAsSb PHOTODIODE RECEIVER

	Dark NEP in 1MHz Bandwidth $W/\sqrt{HZ'}$	NEP With Light $W/\sqrt{HZ'}$	
ITT S-1 Photomultiplier	2.2×10^{-12}	4×10^{-12} (P_1=11.5 nW)	
GE Silicon APD/50Ω preamp receiver	2×10^{-13}	7.5×10^{-13} (P_1=25 nW)	
Science Center GaAsSb photodiode receiver	9.2×10^{-14}	1.16×10^{-13} (P_1=11.5 nW)	2.3×10^{-13} (P_1=25 nW)

depleted region is required because the optical absorption depth of photons of 1.06 μm wavelength is 0.1 cm in Si, an indirect transition material, in contrast to 10^{-4} cm in GaAsSb, a direct transition material. To achieve this wide depletion region in the GE Si diode requires 2500 volts while only 23.5 volts is required to achieve the required depletion width in the Rockwell GaAsSb diode. Moreover, the wide depletion region in the Si APD limits the ultimate frequency response due to the greater transit time. As a result, a photodiode or an avalanche photodiode fabricated from a direct transition material, such as GaAsSb, also has an inherently higher frequency response compared to Si devices.

While the GaAsSb photodiode exhibits superior characteristics over the S-1 photomultiplier and Si APD, its overall performance is well below its theoretical or expected level. In large measure this results because the avalanche gain in GaAsSb diode does not exceed 4. Research of other direct transition ternaries and quaternaries of the III-V materials system has been accelerated. These investigations generally tend to concentrate on obtaining avalanche gains of 10 or greater in p-n homojunctions. The approach to obtaining higher avalanche gain is to fabricate photodiode structures with less lattice mismatch [2]. The GaAlSb ternary shows some promise, but it is in the early research stage [3]. It could be several years before definitive data are obtained showing which ternary is superior.

Because there are many combinations of ternaries and/or quaternaries which show promise in photodiodes and avalanche photodiodes, it will be very costly to investigate all possible combinations in the laboratory and

to determine the optimum combination for a given set of specifications. In order to insure the highest return on investment that future R & D expenditures represent, a study was conducted to develop a comprehensive analytical method that reliably predicts device performance. The study extends the analytical method developed for solar cells to photodiodes. The results of the analytical study and subsequent computer programming were then applied to the photodiode structure under investigation by the Rockwell International Science Center [2,3].

SECTION III

BACKGROUND

Photoenhancement in reverse-biased, nonavalanching p-n junctions was first demonstrated in Ge by Goucher, et al. [4]. For low voltages (i.e., below breakdown), this work showed that within wide limits the spectral response is independent of bias voltage. The same effect is observed in Si reverse-biased p-n junctions. However, it was shown by McKay and McAfee that quantum yields exceed unity at reverse-bias voltages in the region of junction voltage breakdown [5]. This is due to internal gain from avalanche multiplication in the depleted region of the junction. Ge p-n junctions may also show quantum yields exceeding unity, provided the depleted region is sufficiently thick [5]. The structure is commonly referred to as a PIN structure [6]. In optimum structure designs the intrinsic region becomes the active region of the device while the p- and n-regions take on supporting roles [7]. It also determines the frequency response of the device; i.e., the amplitude of the photocurrent decreases while the phase shift between the signal and photocurrent increases with increasing frequency or with increasing depletion width at a given frequency. Spectral response increases with increasing depletion width. Therefore, an engineering optimum must be obtained between high frequency response and high spectral response [7-13].

A photodiode may be made to operate as a wide bandwidth detector provided the real part of the load impedance is kept small [14]. This determines the minimum signal power that the photodiode is capable of detecting and is usually limited by the thermal noise generated in the small load resistance in the absence of internal avalanche multiplication

gain [15,16]. Improved detector sensitivity, while maintaining wide bandwidth, can only be obtained through internal avalanche multiplication gain. Johnson first showed evidence that avalanche multiplication gain can be employed in a wide bandwidth photodiode to assist in overcoming thermal receiver noise and thus improving signal-to-noise ratio [17]. This has generated much interest in avalanche photodiodes. Devices have been fabricated free of microplasmas [18,19], and it has also been substantiated that S/N improves [20,21].

The initial report by Johnson resulted in the development of models to examine the influence of the avalanche gain on bandwidth and S/N. The early models were relatively crude and led to a conclusion that the avalanche photodiode could not be broadbanded [22]. For example, applying the analysis used to study avalanche multiplication in Read diodes [23] showed that avalanche multiplication process limits bandwidth [22]. The assumptions used in the model were that electron and hole ionization coefficients (α and β, respectively) are equal, $\beta/\alpha=1$; electron and hole velocities are equal; and displacement current is small compared to particle current in the avalanche multiplication region and is neglected. Other treatments assumed $\beta=0$, $\beta/\alpha=0$; and concluded that avalanche multiplication had no effect on diode bandwidth [24].

A less restrictive analysis, which did not restrict the ratio β/α, was made [8] using the basic transport equations formulated by Van Roosbroeck [25]. This work showed that when $\beta/\alpha=0$, other parameters have little effect on device bandwidth. Furthermore, when the Lee and Batdorf [22] assumptions are imposed (i.e., $\beta/\alpha=1$ and equal electron and

hole velocities), it was found that the displacement current is small compared to the particle current in the avalanche multiplication region and can be neglected.

Further analytical studies indicate that the ratio β/α also affects the noise power generated in the region in which multiplication occurs [26,27]. When $\beta/\alpha=1$, the multiplication noise power is a function of M_o^3, where M_o is the dc avalanche multiplication gain. Therefore, the signal-to-noise ratio is dependent on M_o^{-1}. Thus, the condition which limits the gain bandwidth also serves to reduce the S/N ratio. However, when $\beta/\alpha=0$, both the noise and signal are dependent on M_o^2, resulting in S/N being independent of M_o. Under these operating conditions, the signal-to-noise ratio and bandwidth are independent of M_o.

The analytical work described above has generally been restricted to the depleted region and, in particular, to that portion of the depleted region in which avalanche multiplication is present. The analysis of a total diode structure has not been reported. While a total diode structure analysis is not likely to give any greater understanding of diode operation for simple structures that may be fabricated from Si and Ge, it may for multilayer structures such as those fabricated from the III-V materials system. Moreover, it is clear that gain bandwidth and S/N are dependent on the ratio β/α and M_o even in simple Si and Ge structures. This dependency requires examination in multilayer structures. Analysis of the total diode structure and the conditions which are more likely to give rise to avalanche multiplication gain along with high gain bandwidth and low S/N will be obtained. In addition, it is important to determine the displacement current in a multilayer diode structure.

SECTION IV

AVALANCHE PHOTODIODE DESIGN CONSIDERATIONS

4.1 Operating Parameters

The ideal receiver in the infrared region of the frequency spectrum combines a low noise preamplifier with an avalanche photodiode. The preamplifier converts the diode photocurrent to a voltage and current suitable for operation into a low resistance (i.e., real part of the load impedance) without degradation of the S/N ratio.

In order to achieve ultimate receiver performance, high performance photodiodes are required. The device characteristics which are capable of being changed and which are critical in achieving high performance diodes are briefly discussed below.

4.1.1 Capacitance

The junction capacitance in conjunction with the preamplifier input stray capacitance of the receiver should be small in order to achieve high frequency response and high S/N. The equivalent R-C circuit determines the cut-off frequency when transit time through the depleted region is short. The noise contribution of the amplifier is linearly proportional to the total input capacitance (i.e., junction plus stray capacitance). The Johnson noise in the photocurrent-sensing resistor is inversely proportional to the square root of the load resistance, which value is determined by the total input capacitance and by the bandwidth required.

4.1.2 Quantum Efficiency

The signal-to-noise ratio in the absence of avalanche multiplication is directly proportional to the quantum efficiency. When the quantum yield (i.e., efficiency) is greater than unity, the S/N ratio

is a complex function of yield. Photodiodes may be fabricated with yields greater than unity. State-of-the-art frequency response dictates that the photons should be absorbed completely within the confines of the depleted region and preferably within the avalanche region of the depleted region. Therefore, the intrinsic layer that forms the depleted region should be fabricated from a direct transition material.

4.1.3 Dark Current

The reverse dark current produced by the externally applied bias arises primarily from three sources. The first is the thermally generated current in the depleted region. The second is the avalanche current produced by the thermal current passing through the avalanche multiplication region, and the third is surface leakage current. The last may be minimized by the application of surface passivation and/or guard ring structures.

4.1.4 Series Resistance

The diode series resistance, which is part of the preamplifier R-C circuit, determines the cut-off frequency when transit time is short. This resistance should be as small as possible. There are two major components which comprise the diode series resistance. The first is the resistance of the semiconductor material sandwiching the intrinsic region. This may be made small by heavily doping these regions and making them thin. The second is the contact resistance at the interface of the metal electrode and the semiconductor. Contact resistance is minimized by using the maximum surface area available for contacting, heavily doping the semiconductor layers to be contacted,

eliminating oxide or insulating layers between the metal electrode and the semiconductor, and by using state-of-the-art general fabrication procedures.

4.1.5 Avalanche Gain

In general, avalanche gain must be sufficient to raise the signal level above preamplifier noise. It has been shown that a gain of 4 to 10 is usually the range over which avalanche photodiodes exhibit a significant improvement in S/N. However, even these modest avalanche gains are difficult to attain. To realize the full potential of avalanche photodiodes fabricated from III-V materials requires a design study to determine those structures and materials which are more likely and those which are less likely to give rise to sufficient gain to overcome preamplifier noise.

4.1.6 Optical Filtering

The signal-to-noise ratio may also be improved through the use of an optical bandpass filter. This serves to greatly reduce the background radiation capable of exciting electrons from the valence to the conduction band. The filter may be applied as a separate component or monolithically incorporated as part of the diode structure. The latter is done by adding a final layer to the diode structure of slightly higher bandgap than the gap of the intrinsic layer.

4.2 Materials Selection

For many applications, Si avalanche photodiodes are more than adequate to satisfy receiver requirements. However, diodes fabricated from an appropriate combination of III-V materials are capable of significantly higher performance characteristics than Si. This arises because material combinations may be selected according to optical transition characteristics,

bandgap value, lattice constant, mobility-field characteristics and lifetime to optimize device design. For example, a direct transition material may be selected for the depletion region in order to effect complete absorption within a thin depletion region. This results in shortened transit time through the depletion region simultaneously with high quantum efficiency. Moreover, many of the III-V binaries, ternaries, and quaternaries have more favorable mobility-field characteristic to reduce depletion region transit time.

The ternaries GaAsSb and GaAlSb are two of the more attractive alloys from which high performance photodiodes have been fabricated. The material properties which may be selected from the GaAsSb and GaAlSb alloys and which are critical in fabricating high performance diodes are briefly discussed below.

4.2.1 Alloy Composition

Multilayer devices may be designed with two or more layers having different bandgap values for the purpose of obtaining filtering, bandedge discontinuities to influence carrier transport and for lattice matching. These alloys may generally be grown selectively with different bandgaps by changing the alloy composition. However, GaAsSb exhibits a miscibility gap between 40 to 70% GaAs mole fraction. This miscibility gap does not prevent the fabrication of photodiodes since the GaAs mole fraction required for the layers is greater than 83%.

4.2.2 Bandgap

Both GaAsSb and GaAlSb may be selectively grown with bandgap values in the 1.064 μm region. Therefore, multibandgap devices may be fabricated from either alloy system.

4.2.3 Lattice Constant

In some cases, lattice misfit and the effects derived therefrom may degrade device performance. While the bandgap vs. lattice constant is linear for GaAlSb, it is not for GaAsSb. The GaSb-rich terminal point of the latter exhibits a trough in bandgap and then increases to the 1.43 eV value at the GaAs-rich terminal point. Moreover, Table 2 shows that the lattice constant change with respect to bandgap is more than one order of magnitude greater in GaAsSb than in GaAlSb. Therefore, in those cases in which interfacial recombination influences device performance, GaAlSb is preferred.

TABLE 2

BANDGAP AND LATTICE CONSTANT FOR THE III-V BINARIES USED IN PHOTODIODE FABRICATION

Binary	Bandgap eV	Lattice Constant Å	% Change in Lattice	
GaSb	0.73	6.095	7.5%	
GaAs	1.43	5.653		0.65%
AlSb	1.65	6.135		

4.2.4 Optical Transition Characteristic

One requirement to fabricate a high cut-off frequency diode with high quantum efficiency is that the depletion region be a direct transition material. This results in more than 63% of the photon flux

being absorbed in approximately 1 μm thick layer, rather than 10^3 μm, in Si devices. It is also required that the layers between the surface and the intrinsic layer be fabricated from larger bandgap and/or indirect transition materials. This insures that there is no significant absorption of the signal photon flux outside of the depletion layer. The ternary GaAsSb is a direct transition alloy over its entire compositional range. Therefore, in the design of a photodiode the layers between the surface and intrinsic layer must be of a larger bandgap value than the intrinsic region. On the other hand, GaAlSb is a direct transition material at the GaSb-rich terminus and indirect at the AlSb-rich terminus. Therefore, diodes may be designed with either thin indirect transition layers and/or wider bandgaps.

4.2.5 Velocity-Field Characteristic

In high cut-off frequency diodes the velocity-field characteristic in the depletion region is of great importance, in addition to the optical transition characteristic. There has not been extensive investigation of this characteristic in GaAsSb and GaAlSb. However, there is reason to believe that the limiting velocity is higher than it is for Si.

4.2.6 Lifetime

In direct transition materials with reasonable crystalline perfection, lifetime is a result of the spontaneous radiative recombination process in the absence of induced or stimulated emission. Typically, in III-V direct transition materials the radiative recombination lifetime at 300°K and $10^{17} cm^{-3}$ impurity concentration is less than 1 μsec. In intrinsic layers where the doping is usually 10^{15} cm^{-3}

or less, the radiative lifetime may be higher. It is unlikely that a sufficient concentration of imperfections may be introduced to lower the effective lifetime below the radiative recombination level. Moreover, transit times in direct transition depletion regions are typically of the order of 10^{-10} sec. This is several orders of magnitude less than the radiative lifetime. Therefore, the collection efficiency of the depletion layer will always be unity in the absence of avalanche multiplication. When avalanche gain is present, the quantum yield will always be greater than unity.

4.3 Diode Structure

The diode described in this section is denoted as the inverted homo-heterojunction by Rockwell International. Figure 1(a) shows the physical schematic structure, and Figure 1(b) shows the deduced band structure. The diode structure in Figure 1 has improved avalanche gain due to the reduction of microplasmas. Earlier structures resulted in the avalanching occurring at a p-n heterojunction (i.e., an n^- region of $GaAs_{0.83}\ Sb_{0.17}$ and a p^+ region of $GaAs_{0.88}\ Sb_{0.12}$). Avalanching should have occurred at the n^-- p^+ heterojunction interface. However, it was surmised that because of lattice defects resulting from lattice misfit, microplasmas were present, and avalanche gain was not observed. In Figure 1 avalanching should occur at the n^-- p^+ homojunction where the lattice mismatch is zero and should be relatively free of lattice defects. Consequently, microplasmas have been reduced and avalanche gain observed. However, the gain has been too low to show marked improvement over the non-avalanche mode of operation. The suggestion has been made that perhaps the lattice misfit present at interfaces X_1

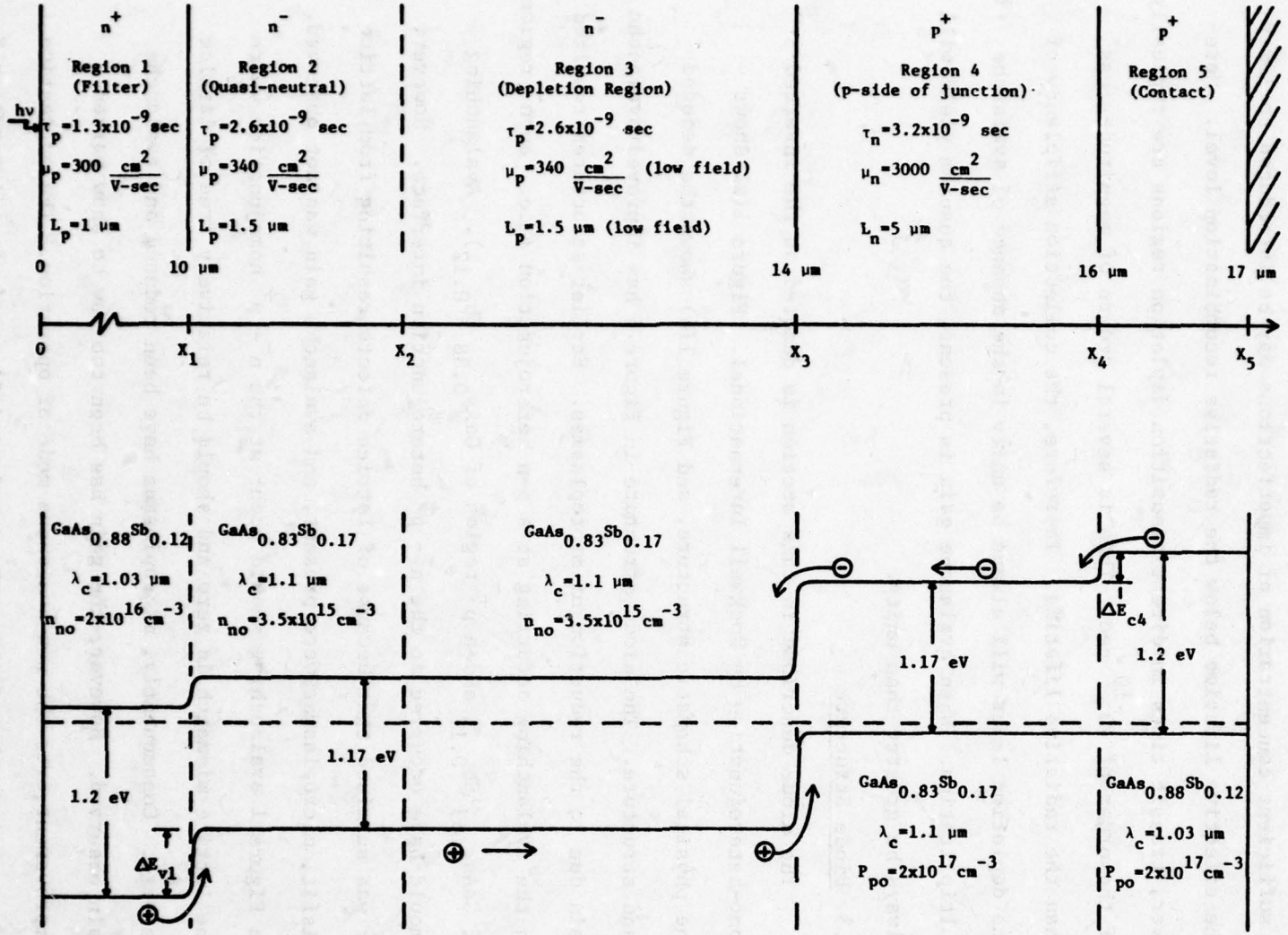

Figure 1. Rockwell International GaAsSb Avalanche Photodiode Band Structure

and X_4 may propagate lattice defects to interface X_3 or the lattice defects at X_1 and X_4 may influence carrier transport which produce microplasmas and restricts avalanche gain.

In Figure 1 the radiation enters the device through the n^+ layer, Region 1, which is 10 μm thick in devices that have been fabricated. The bandgap of this layer is 1.2 eV and is composed of the ternary $GaAs_{0.88}\ Sb_{0.12}$. It is 30 meV wider than the p-n homojunction materials. Region 1 serves as an optical filter to minimize background radiation from entering the diode active regions. Since its bandgap is 30 meV wider than Region 3 and if free carrier absorption is small, the radiation carrying the signal will pass through this layer unattenuated.

Region 2 is the undepleted n^- layer. In well-designed diodes the depleted region extends through Region 2, resulting in $X_1=X_2$.

The depleted layer is designated Region 3. Its bandgap is 1.17 eV and is composed of the ternary $GaAs_{0.83}\ Sb_{0.17}$. It is a direct transition alloy. Almost all of the photons of the signal radiation will be absorbed in a thickness 1 to 4 μm, depending on its line width and its precise location in the infrared spectrum.

Region 4, the p^+ layer, serves as the p-side of the p-n homojunction. Ideally, the photon flux entering Region 4 should be small. If it is not small the diode structure is not optimized and the frequency response may be low due to the diffusion carrier transport mechanism which takes place in this layer.

Region 5 is a more heavily doped region to which an ohmic contact is made to obtain low contact resistance.

SECTION V

ANALYSIS AND RESULTS

In this section the analysis is referred to only where required to fully discuss the results. The material and structural input parameters are given in Figure 1 and were obtained from Dr. James Harris, Rockwell International.

The assumptions used in the analysis were fully described in the Final Report (Contract No. F33615-76-C-1283) and will not be repeated here.

The received radiant energy is assumed to have a spectrum similar to an LED represented by the Gaussian function.

$$N = (1-R)\, N_o e^{-\zeta(\lambda-\lambda o)^2} \tag{1}$$

where the reflectance is taken to be constant or

$$R = 0.05 \tag{2}$$

and

$$\lambda_o = 1.064\ \mu m\ (1.165\ eV), \tag{3}$$

$$\zeta = 4.44 \times 10^3 \tag{4}$$

and where the line width is

$$2\Delta\lambda_1 = 250\ \mathring{A}\ . \tag{5}$$

The total photon flux chosen is

$$\int_{1.052}^{1.077} (1-R)N_o e^{-4.44\times10^3(\lambda-\lambda_o)^2} d\lambda = 2.528\times10^{13} cm^{-2}sec^{-1}. \tag{6}$$

This results in a maximum current density value

$$J_{max} = 1.6 \times 10^{-19} \times 2.528 \times 10^{13}$$

$$= 4.04 \times 10^{-6} \text{ amps cm}^{-2}. \qquad (7)$$

The incident power density is approximately 4.5 mWatts cm^{-2}. The diode mesa is taken to be 4 mils in diameter or 7.9×10^{-5} cm^2 in area. This results in an incident power on the diode of approximately 0.35 nWatt. The maximum diode current is approximately 0.3 nAmp.

To fully deplete the n^- region requires -43 volts reverse bias. At a reverse voltage of -40 volts, the depletion layer is 3.9 μm.

The results of the first set of calculations given in Figures 2(a) to 2(g) show the total spectral response and the components making up the total when the filter layer, Region 1, is varied in thickness from 1 μm to 15 μm. The response curves labeled Regions 1 + 2 and Region 3 are the contributions to the total response due to excess holes generated by absorbed photons. Similarly, the curve labeled Regions 4 + 5 are for electrons. Unless otherwise stated, when the n^- region is fully depleted, Region 2 is always 0.1 μm thick. As a result, when n^- is fully depleted the curve labeled Regions 1 + 2 is the response of Region 1 for all practical purposes in these curves. As these calculations show, when the filter thickness, Region 1, is thin, its contribution to spectral response is appreciable. As shown in Figure 2(a), it is in excess of 40% for wavelengths less than 1.05 μm for 1.0 μm thickness. The response for Region 1 cuts off sharply in the region 1.035 μm due to its wavelength cut-off arising from its bandgap. A large

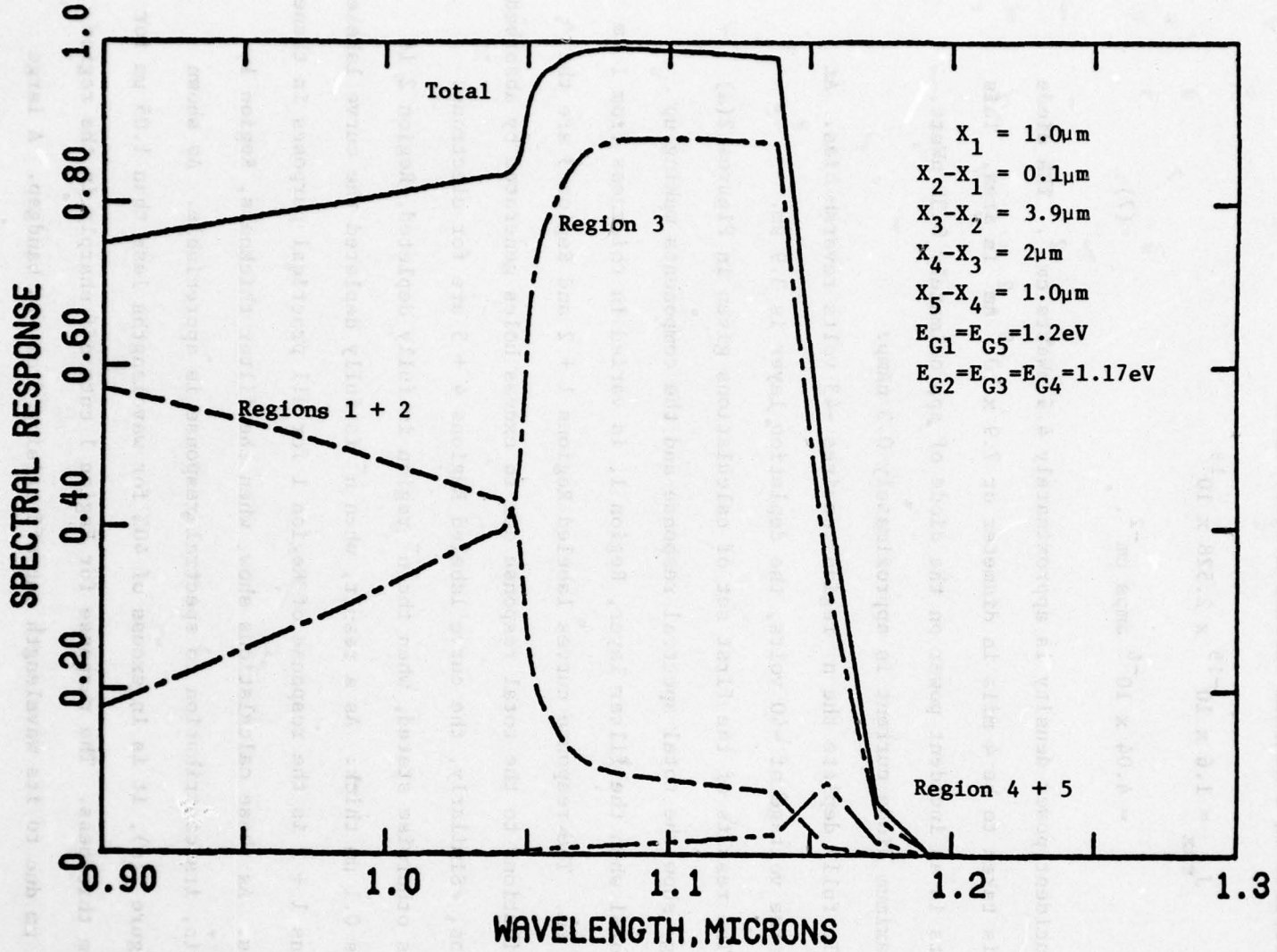

Figure 2(a). Photodiode spectral response in non-avalanche mode for X_1 = 1.0 μm.

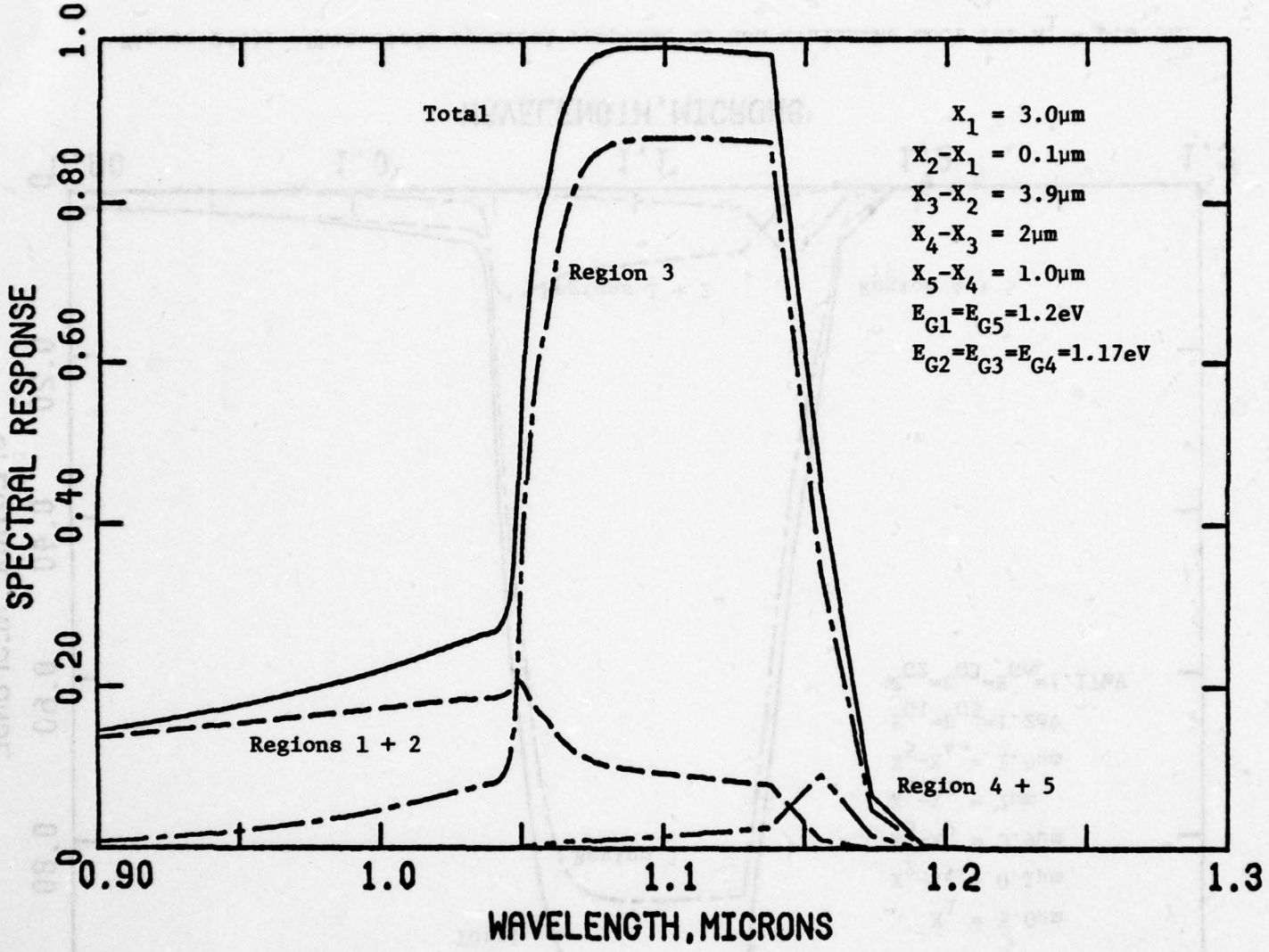

Figure 2(b). Photodiode spectral response in non-avalanche mode for X_1 = 3.0 μm.

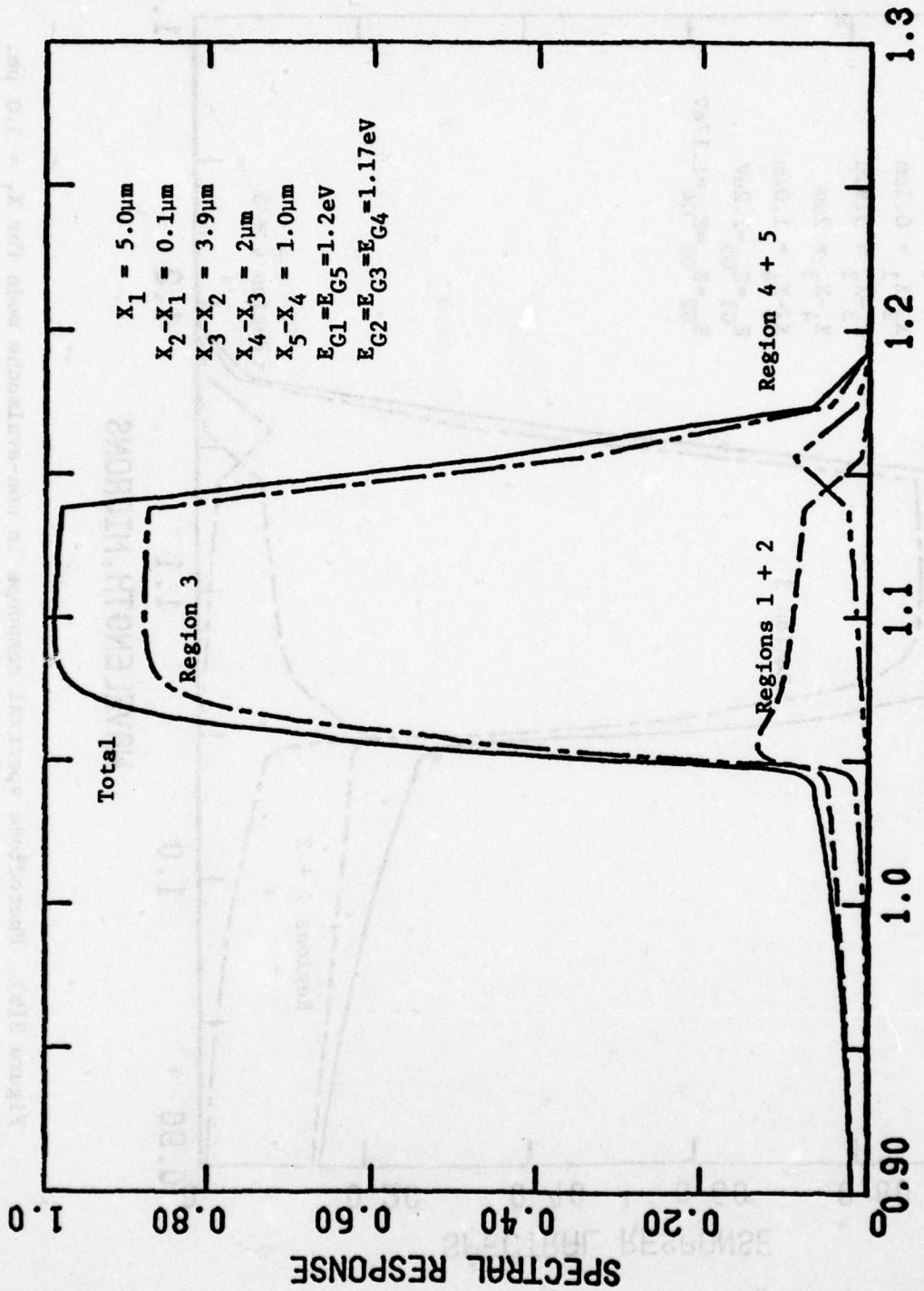

Figure 2(c). Photodiode spectral response in non-avalanche mode for X_1 = 5.0 μm.

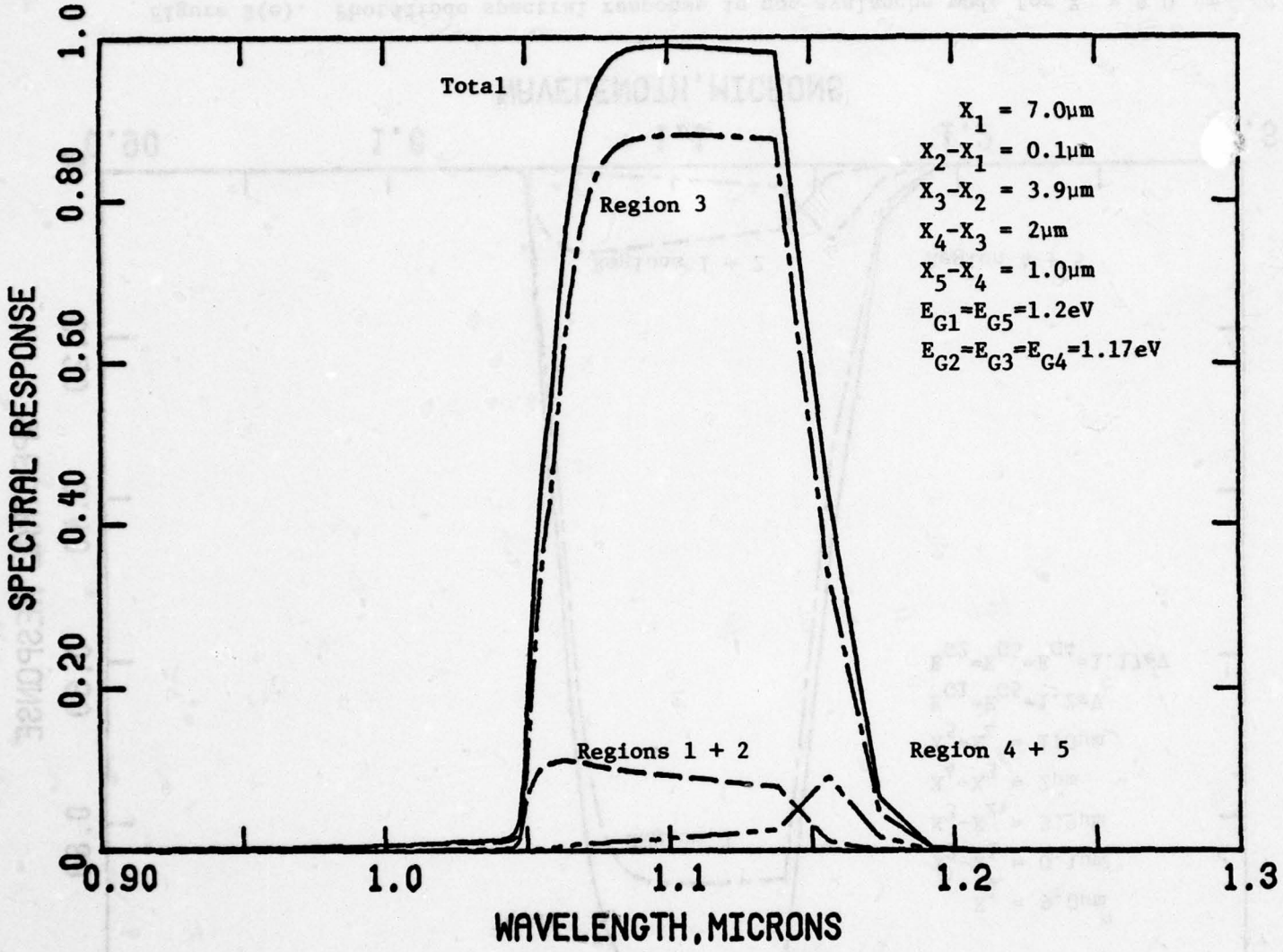

Figure 2(d). Photodiode spectral response in non-avalanche mode for X_1 = 7.0 μm.

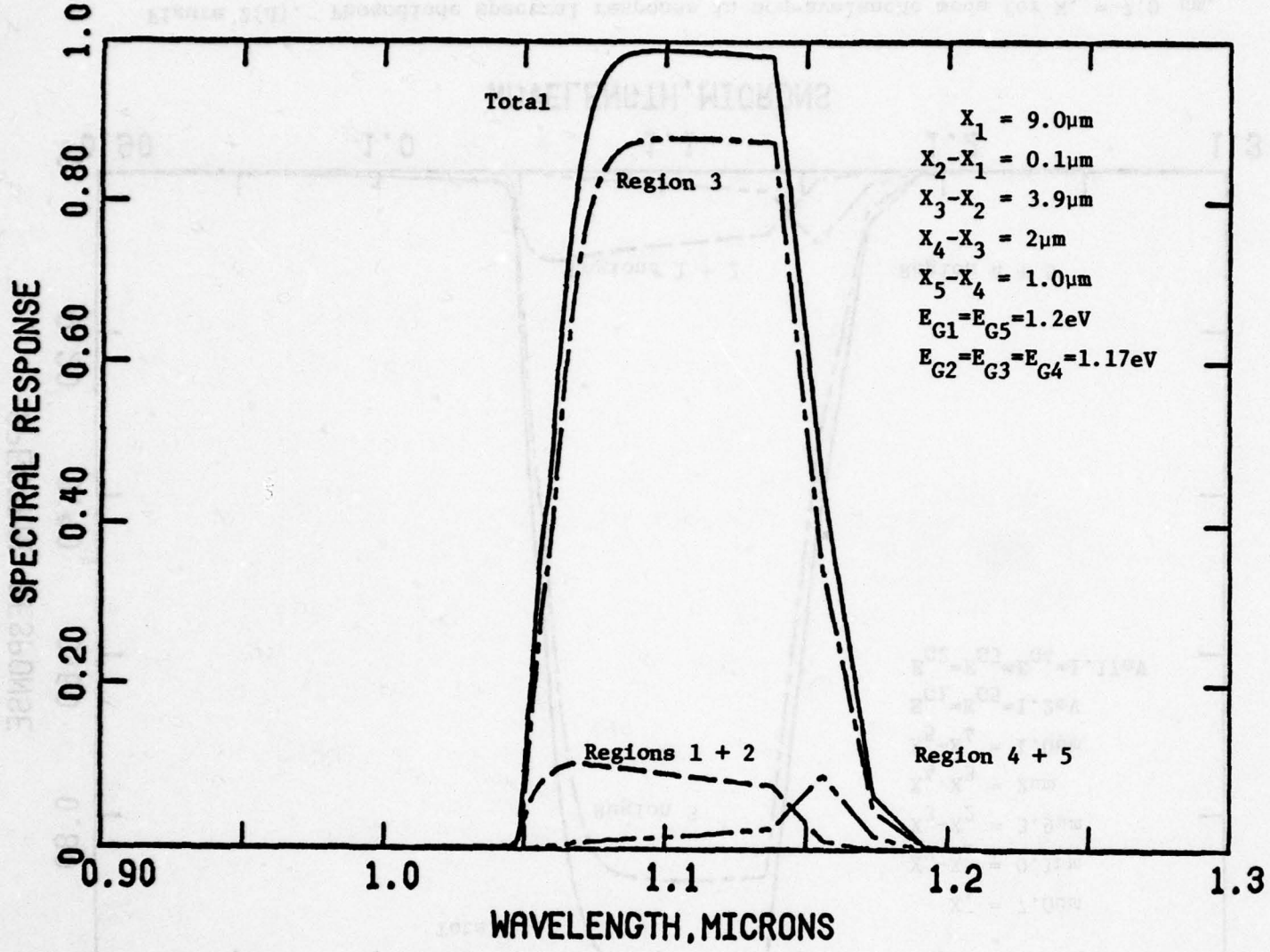

Figure 2(e). Photodiode spectral response in non-avalanche mode for X_1 = 9.0 μm.

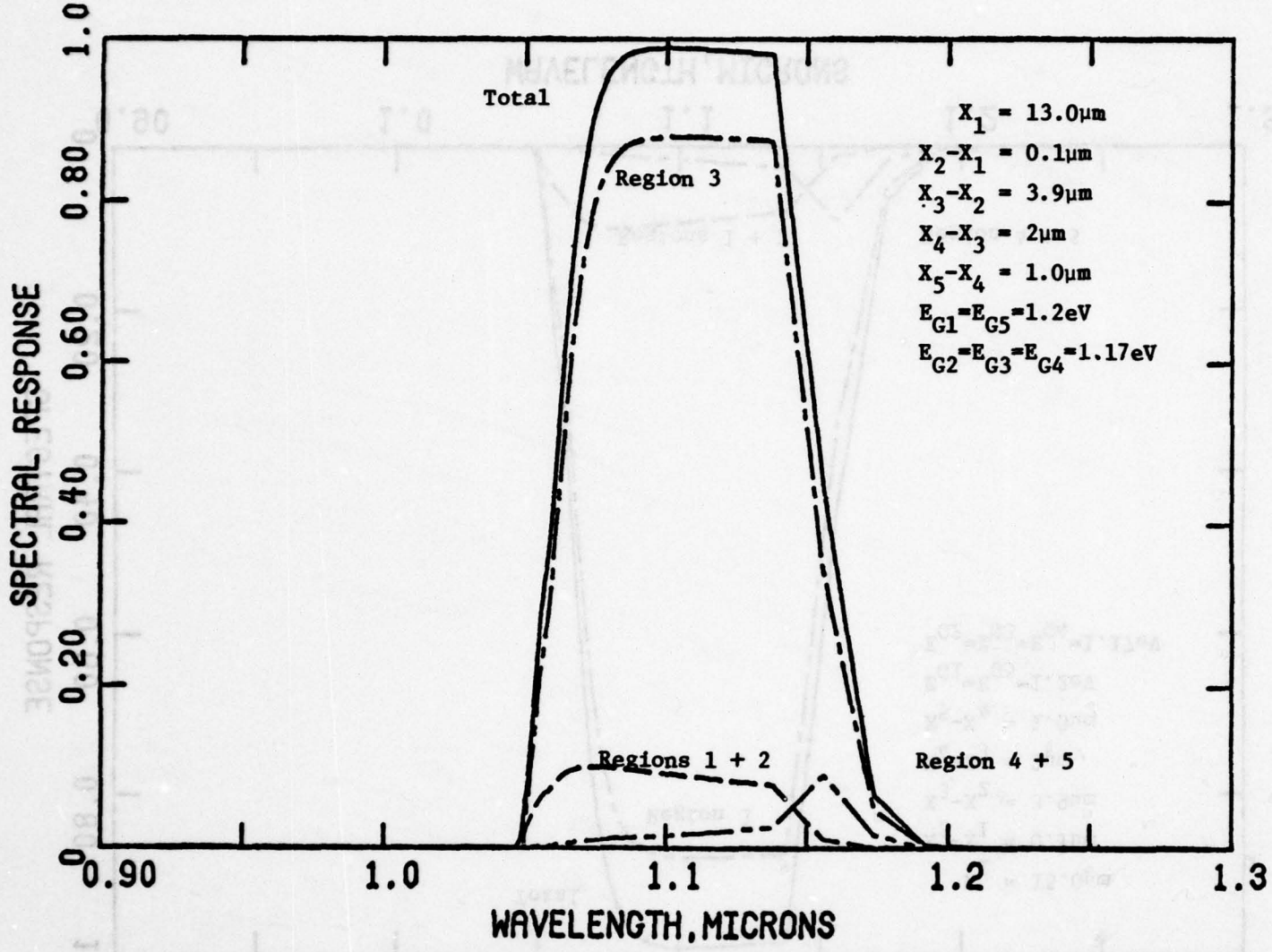

Figure 2(f). Photodiode spectral response in non-avalanche mode for X_1 = 13.0 μm.

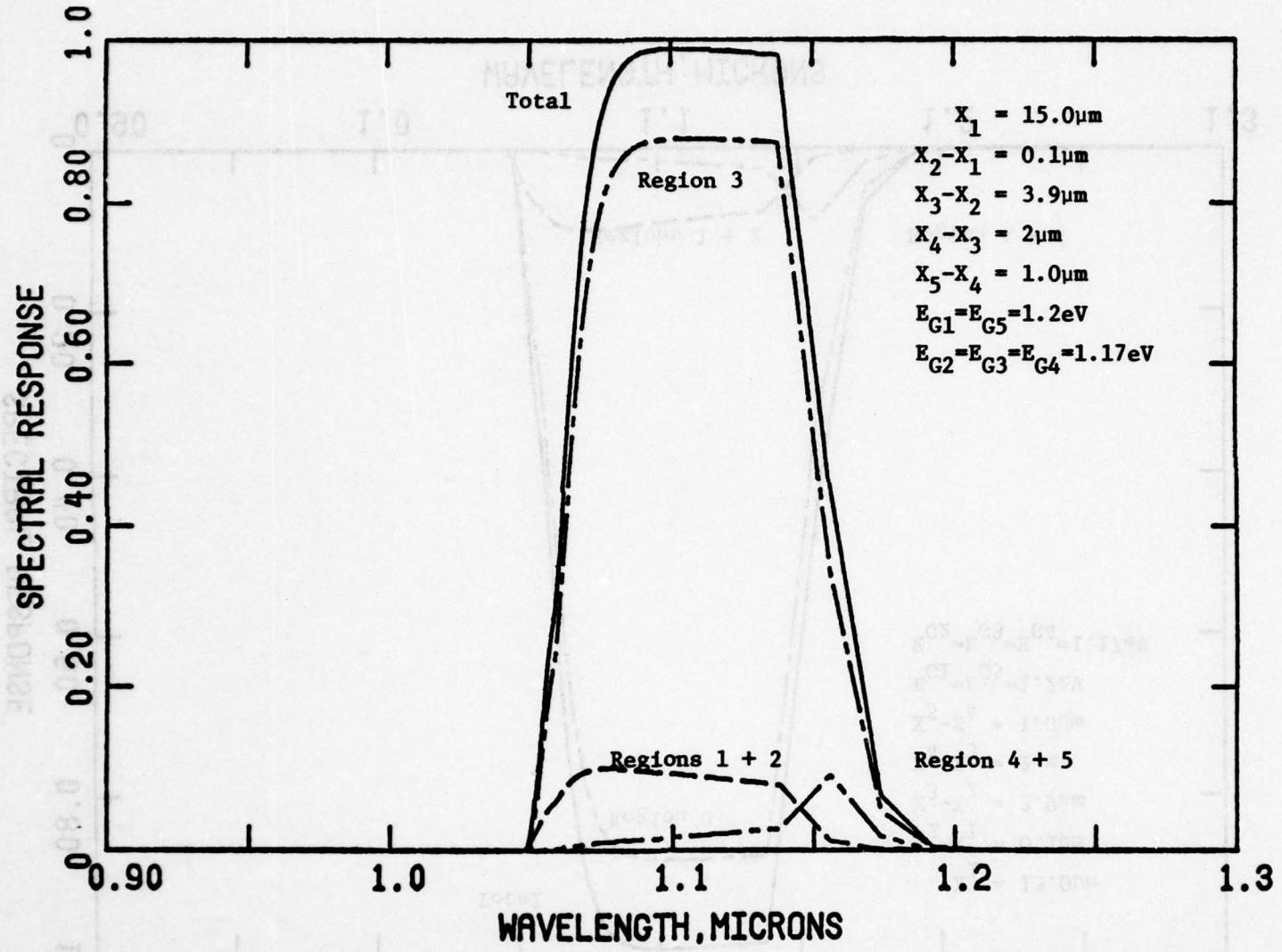

Figure 2(g). Photodiode spectral response in non-avalanche mode for X_1 = 15.0 μm.

fraction of the holes generated in this region enter Regions 2 and 3 and are collected by the junction since the hole diffusion length is 1 μm, thereby contributing to the total spectral response. For filter thickness values greater than 1 μm, the hole response in Region 1 decreases rapidly. For 7.0 μm filter thickness the hole response is negligible at wavelengths less than 1.05 μm. The hole response in the spectral range 1.05 to 1.15 μm is due to Region 2 which has a thickness of 0.1 μm. There is essentially no change in the response in this range even up to 15.0 μm thickness for Region 1.

While there is no change in the tailing (high wavelength) edge of the total spectral response, in the Region 3 response contributed by holes, or in peak value, there is a spectral narrowing in these response curves as the filter thickness increases. Thus, it is seen that the filter is performing the function of filtering high energy photons, such as exists in the background, thereby serving to improve S/N.

The hole contribution to spectral response in Region 1 is not desirable with respect to frequency response considerations. For optimum design the filter should be of sufficient thickness, in conjunction with its hole diffusion length, to affect a negligible contribution to spectral response as well as to filter out background radiation on the short wavelength side. These calculations show that a thickness of 7.0 μm is sufficient for a 1 μm hole diffusion length to accomplish this.

The spectral range in which the signal carrier resides is from 1.052 to 1.077 μm (i.e., the 3 db points). In this spectral range the hole spectral response contributed by the depleted region remains nearly constant

for the range of X_1 studied in the absence of free carrier absorption in Region 1. The signal photon flux distribution through the photodiode structure is shown in Figure 3 corresponding to the spectral response curves presented in Figure 2(b) for a 3 μm filter thickness. The curve shows that approximately 5% of the signal photon flux is absorbed in the filter layer. This calculation shows that thin filter layers may increase S/N through a reduction in the absorption of the signal photon flux in this layer. We conclude that thin filter layers may be employed provided that the hole lifetime is sufficiently reduced so that the hole diffusion length becomes much smaller than the filter thickness.

Figure 4 [3a] is spectral response experimental data reported on a 5 mil diameter GaAsSb photodiode. The voltage to fully deplete appears to be in the range of 50 to 70 volts. The spectral response curve represented in Figure 2(b) shows agreement with the response in the spectral region from 1.05 to 1.15 μm to within approximately 5%. At shorter wavelengths the experimental data show the cut-off to occur at 0.98 μm rather than at 1.05 as shown in Figure 2(b). This may be attributed to the bandgap of the filter layer being 1.26 eV rather than 1.2 eV as shown in Figure 2(b). The cut-off at long wavelengths is at approximately 1.15 eV for both the experimental and calculated curves. This reflects the bandgap cut-off of the depleted region being 1.17 eV for both cases. Thus, the calculated spectral response gives fairly good agreement with experimental data.

Figures 5(a) through 5(g) show the influence of reverse bias on spectral response. The signal carrier photon flux distribution throughout

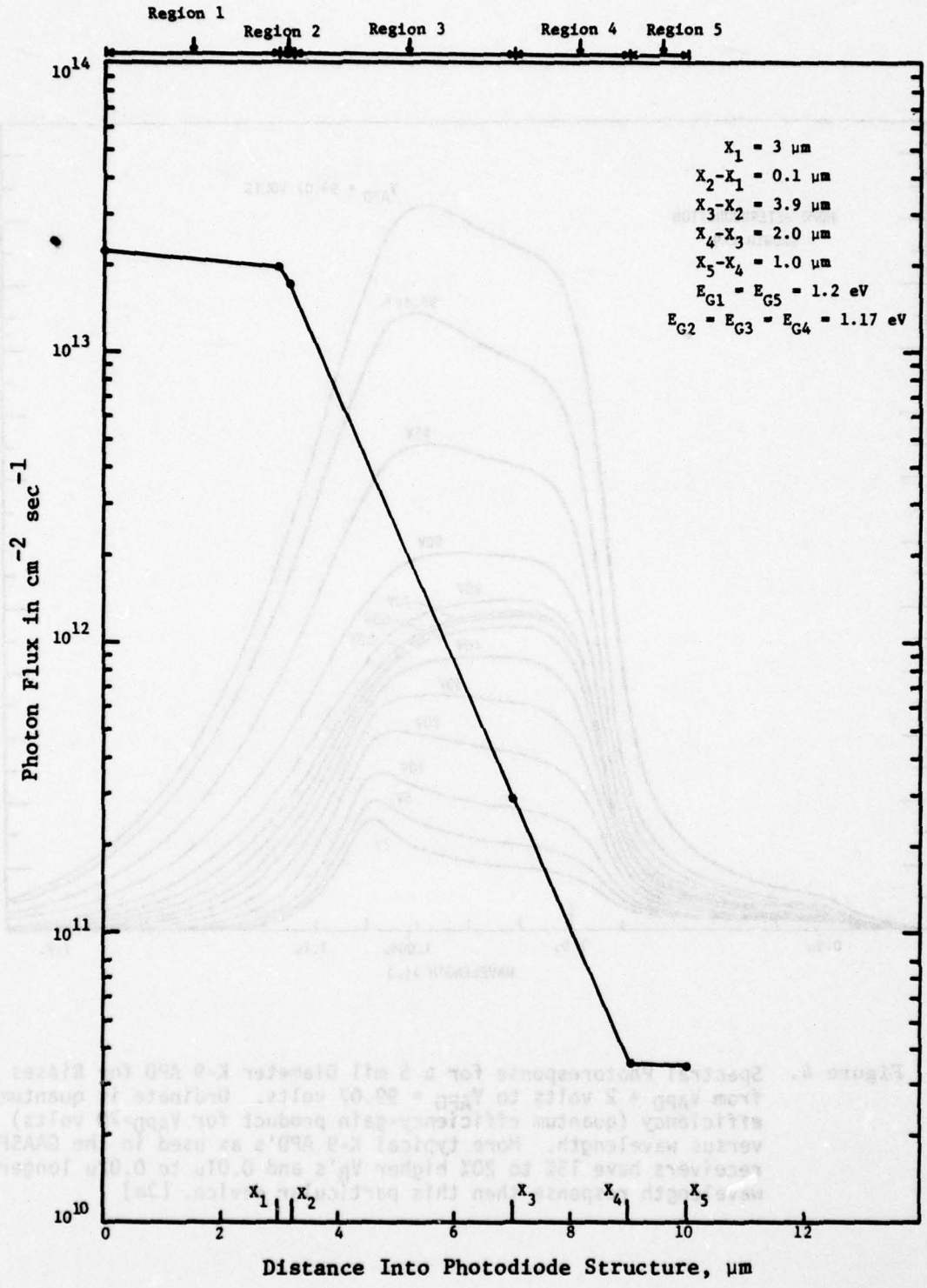

Figure 3. Signal photon flux distribution through the photodiode structure.

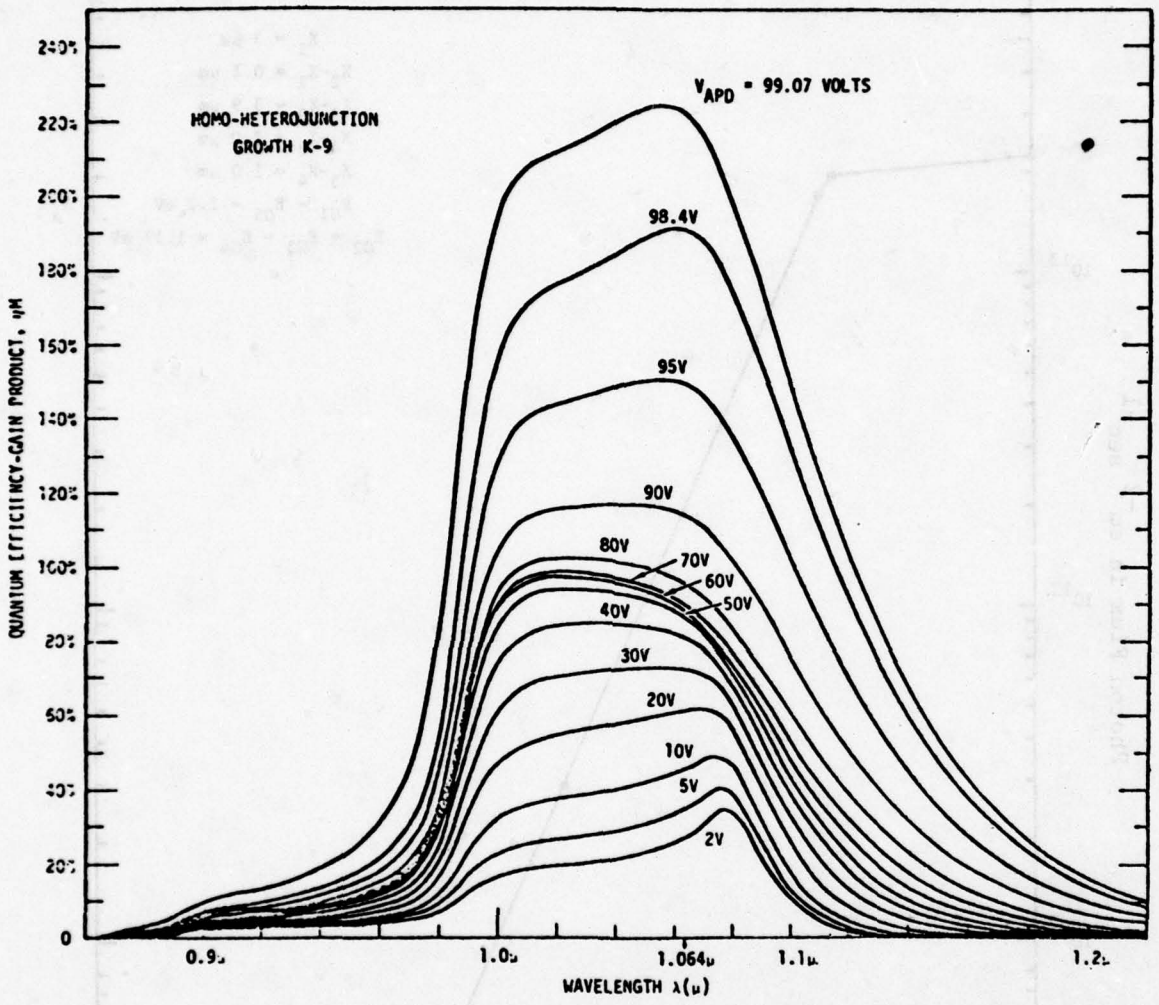

Figure 4. Spectral Photoresponse for a 5 mil Diameter K-9 APD for Biases from V_{APD} = 2 volts to V_{APD} = 99.07 volts. Ordinate is quantum efficiency (quantum efficiency-gain product for V_{APD}>70 volts) versus wavelength. More typical K-9 APD's as used in the GAASFET receivers have 15% to 20% higher V_B's and 0.01μ to 0.02μ longer wavelength response than this particular device. [3a]

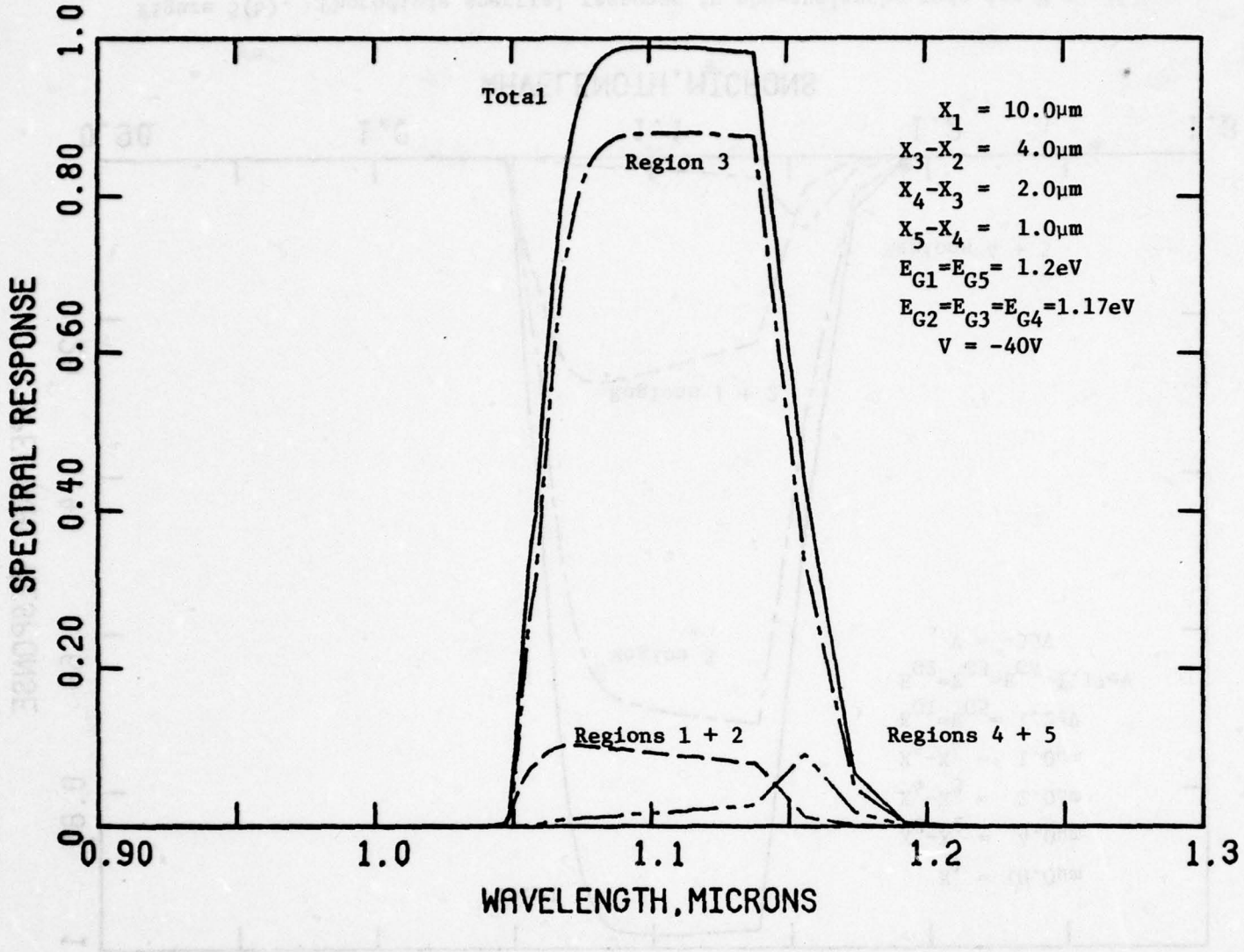

Figure 5(a). Photodiode spectral response in non-avalanche mode for V = -40 V.

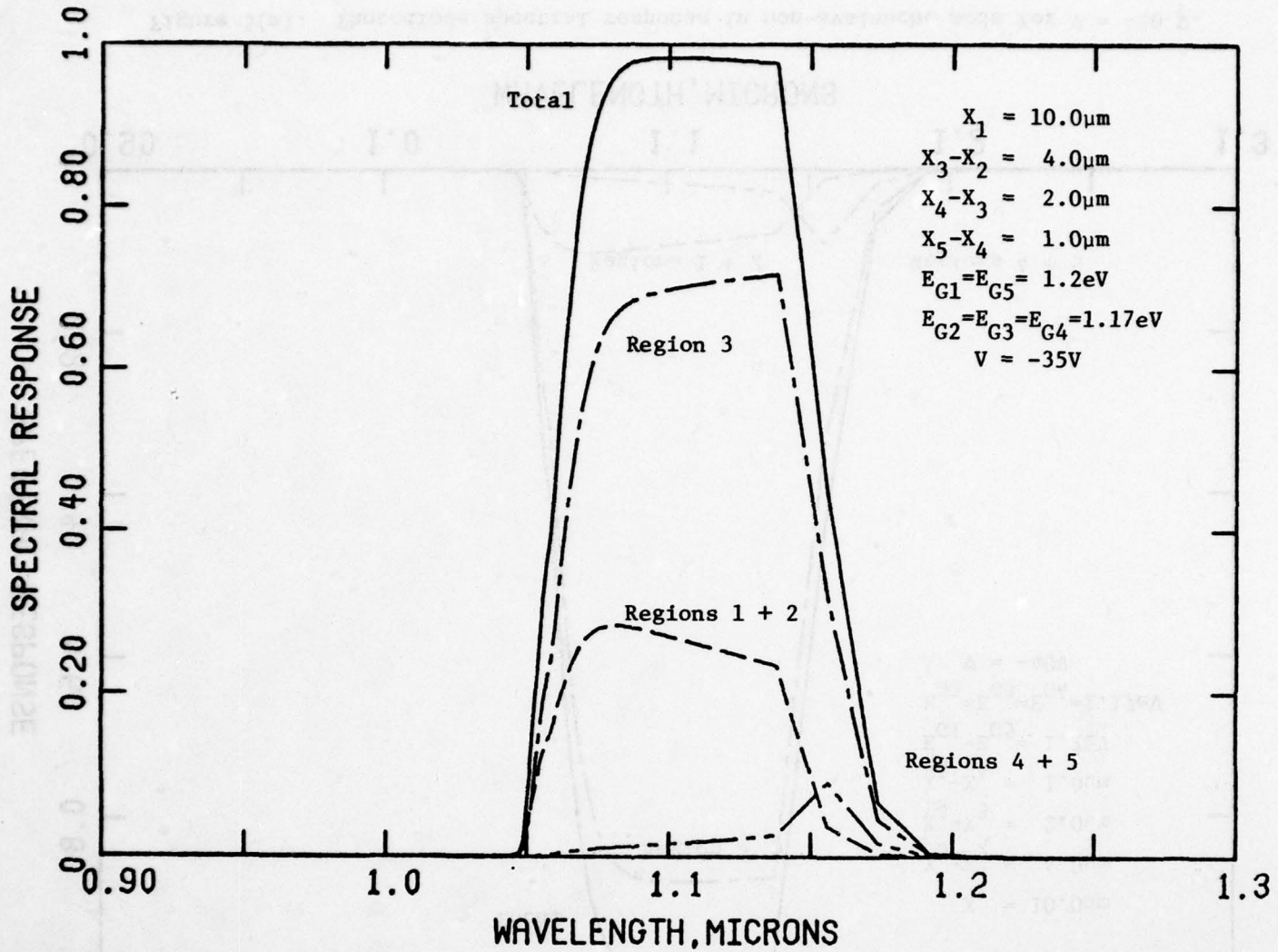

Figure 5(b). Photodiode spectral response in non-avalanche mode for V = -35 V.

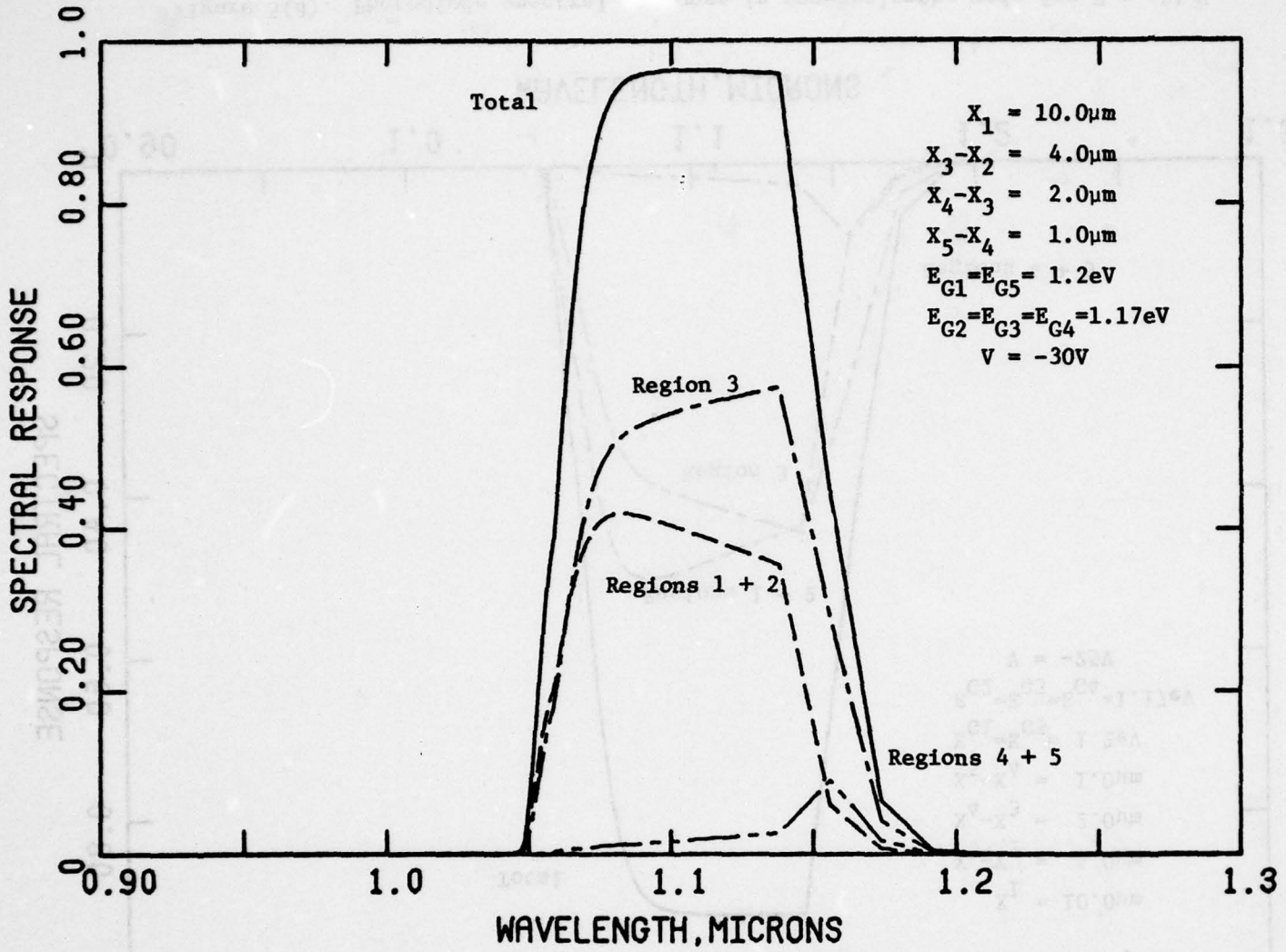

Figure 5(c). Photodiode spectral response in non-avalanche mode for V = -30 V.

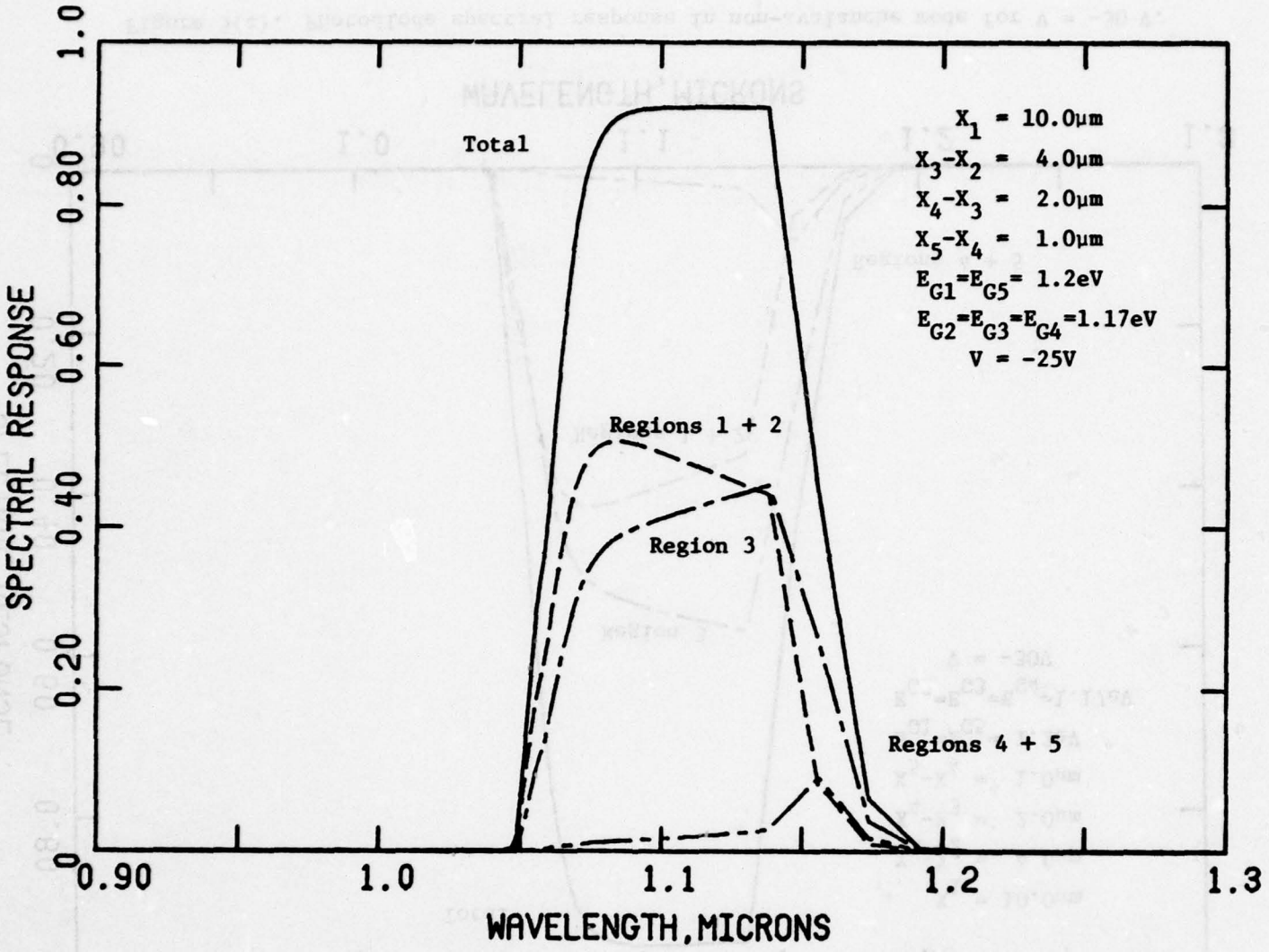

Figure 5(d). Photodiode spectral response in non-avalanche mode for V = -25 V.

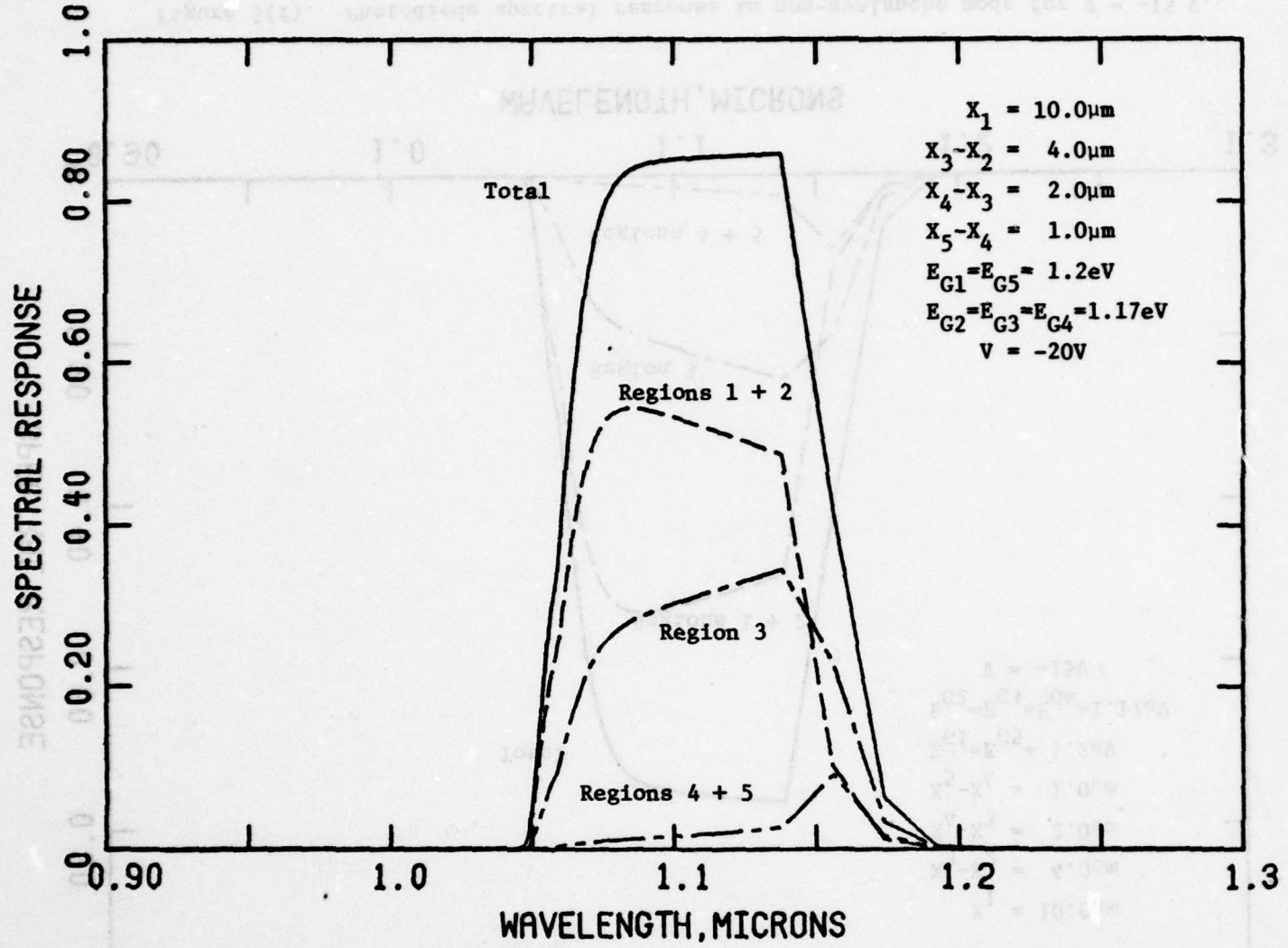

Figure 5(e). Photodiode spectral response in non-avalanche mode for V = -20 V.

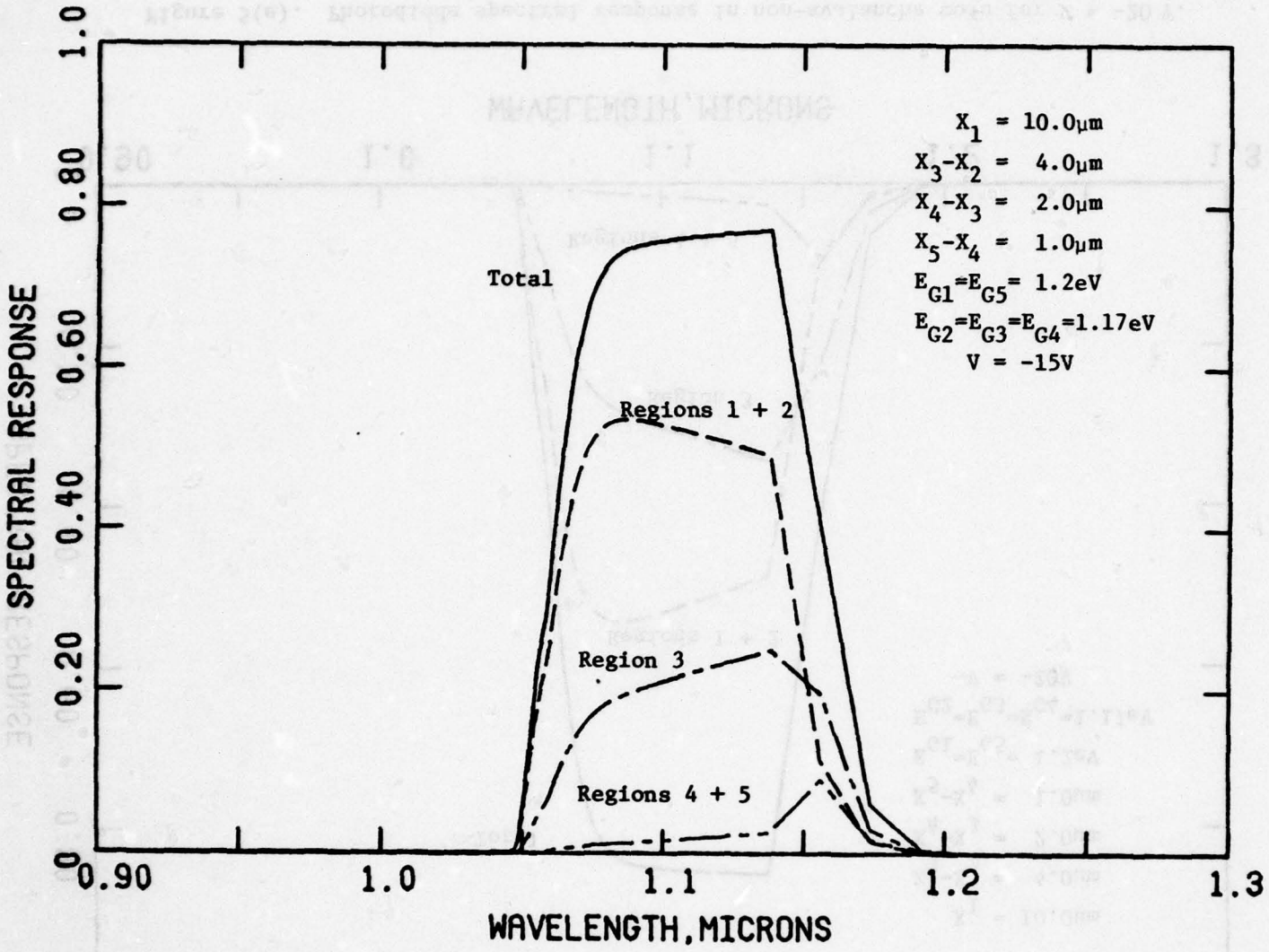

Figure 5(f). Photodiode spectral response in non-avalanche mode for V = -15 V.

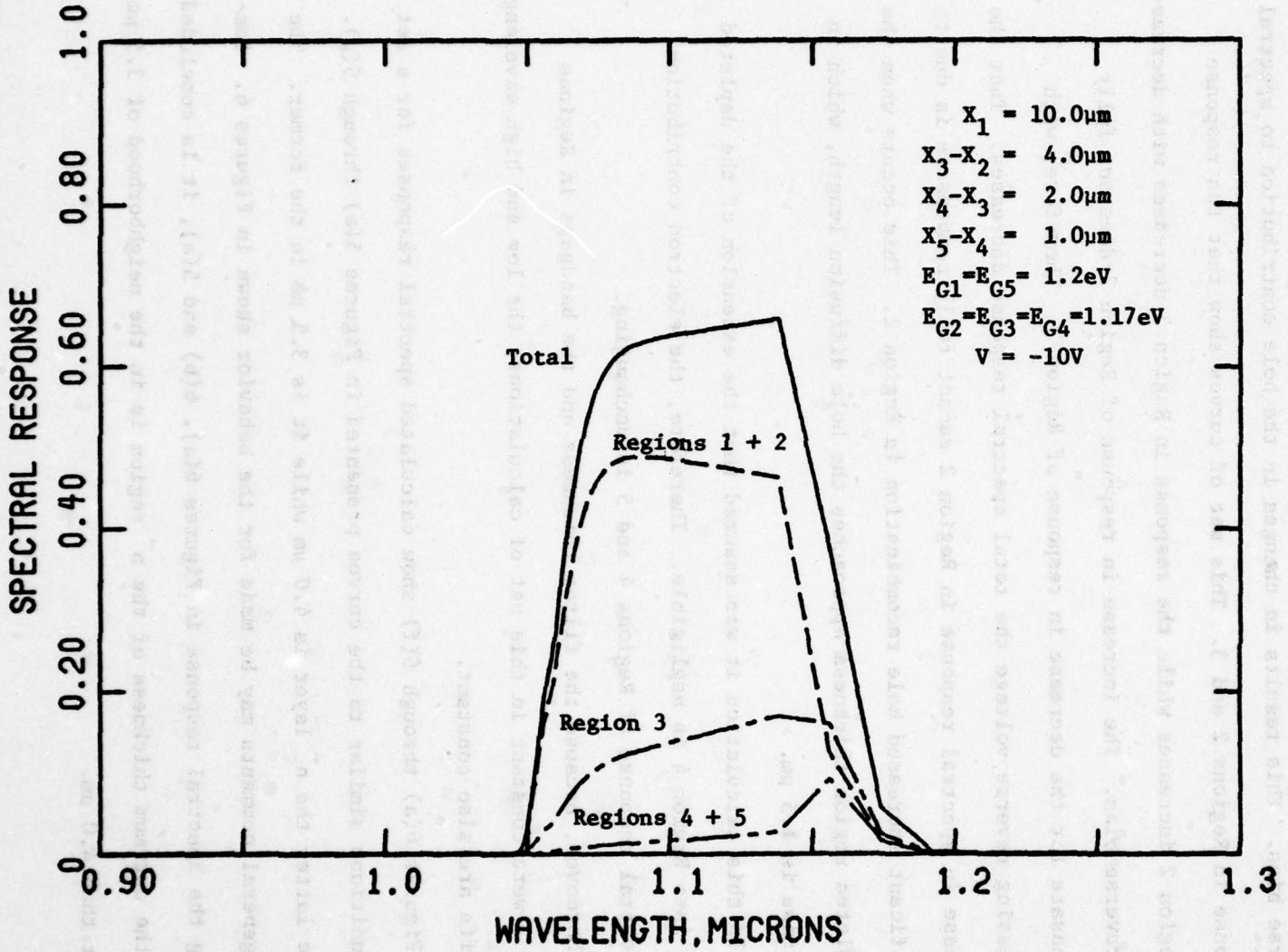

Figure 5(g). Photodiode spectral response in non-avalanche mode for V = -10 V.

the structure does not change. However, X_2-X_1 and X_3-X_2 both change with reverse bias. This results in changes in the hole contribution to spectral response in Regions 2 and 3. This set of curves show that the response in Region 2 increases while the response in Region 3 decreases with decreasing reverse bias. The increase in response of Region 2 does not fully compensate for the decrease in response of Region 3. Therefore, with decreasing reverse voltage the total spectral response decreases. That the increase in spectral response in Region 2 cannot fully compensate is due to significant increased hole recombination in Region 2. This occurs when the undepleted region thickness approaches the hole diffusion length, which in this case is 1.5 μm.

In this calculation it was assumed that the extension of the depleted layer into Region 4 is negligible. Therefore, the electron contribution to spectral response of Regions 4 and 5 is unchanging.

Moreover, because the filter thickness and the bandgaps in Regions 2 and 3 were constant in this set of calculations, the low and high wavelength cut-offs are also constant.

Figures 6(a) through 6(f) show calculated spectral responses for a set of conditions similar to the curves presented in Figures 5(a) through 5(g). In the latter the n^- layer is 4.0 μm while it is 3.5 μm in the former. The same general comments may be made for the behavior shown in Figures 6. Comparing the spectral response in Figures 6(a), 6(b) and 5(a), it is concluded that the optimum thickness of the n^- region is in the neighborhood of 3.5 μm rather than 4.0 μm.

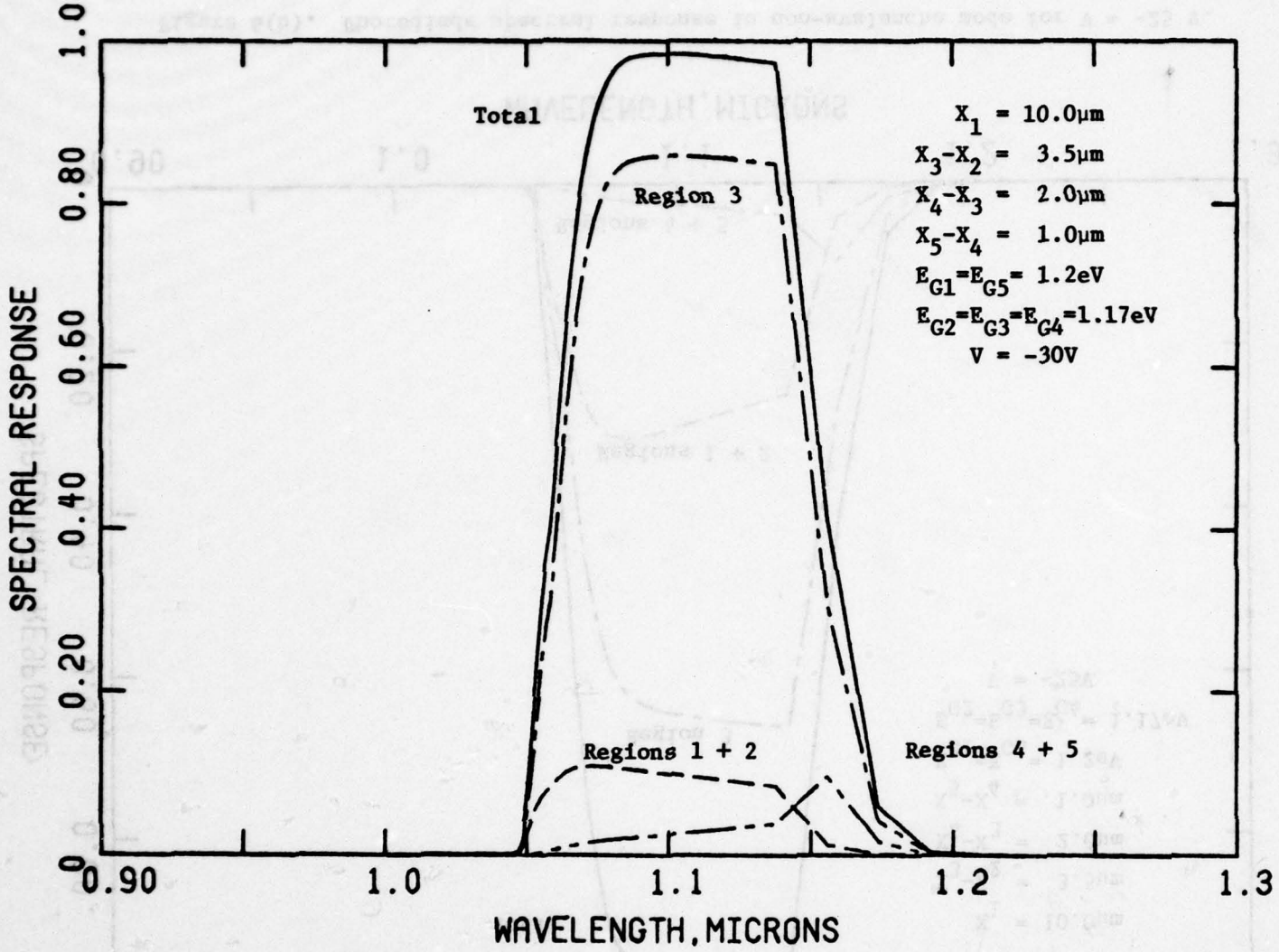

Figure 6(a). Photodiode spectral response in non-avalanche mode for V = -30 V.

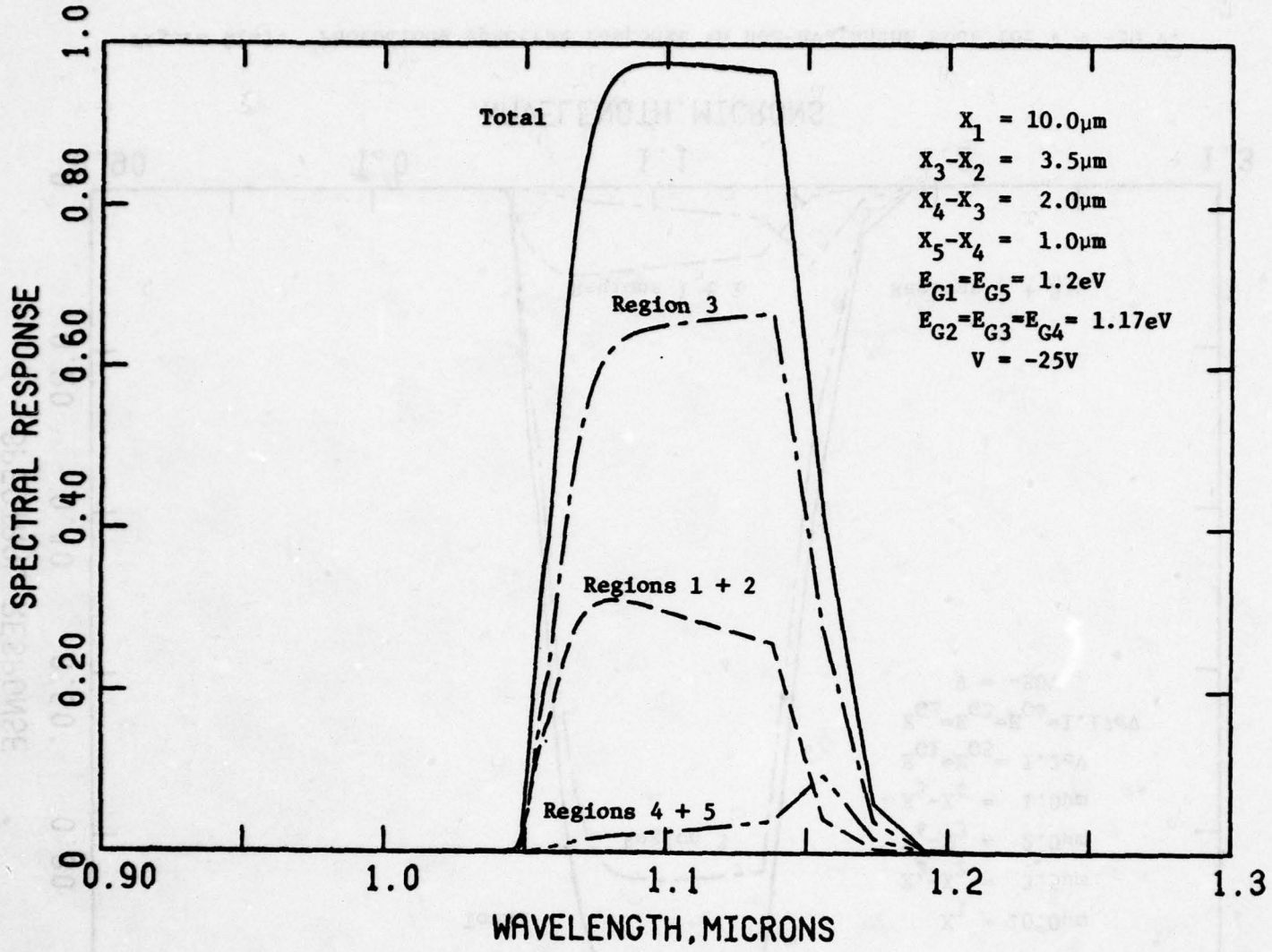

Figure 6(b). Photodiode spectral response in non-avalanche mode for V = -25 V.

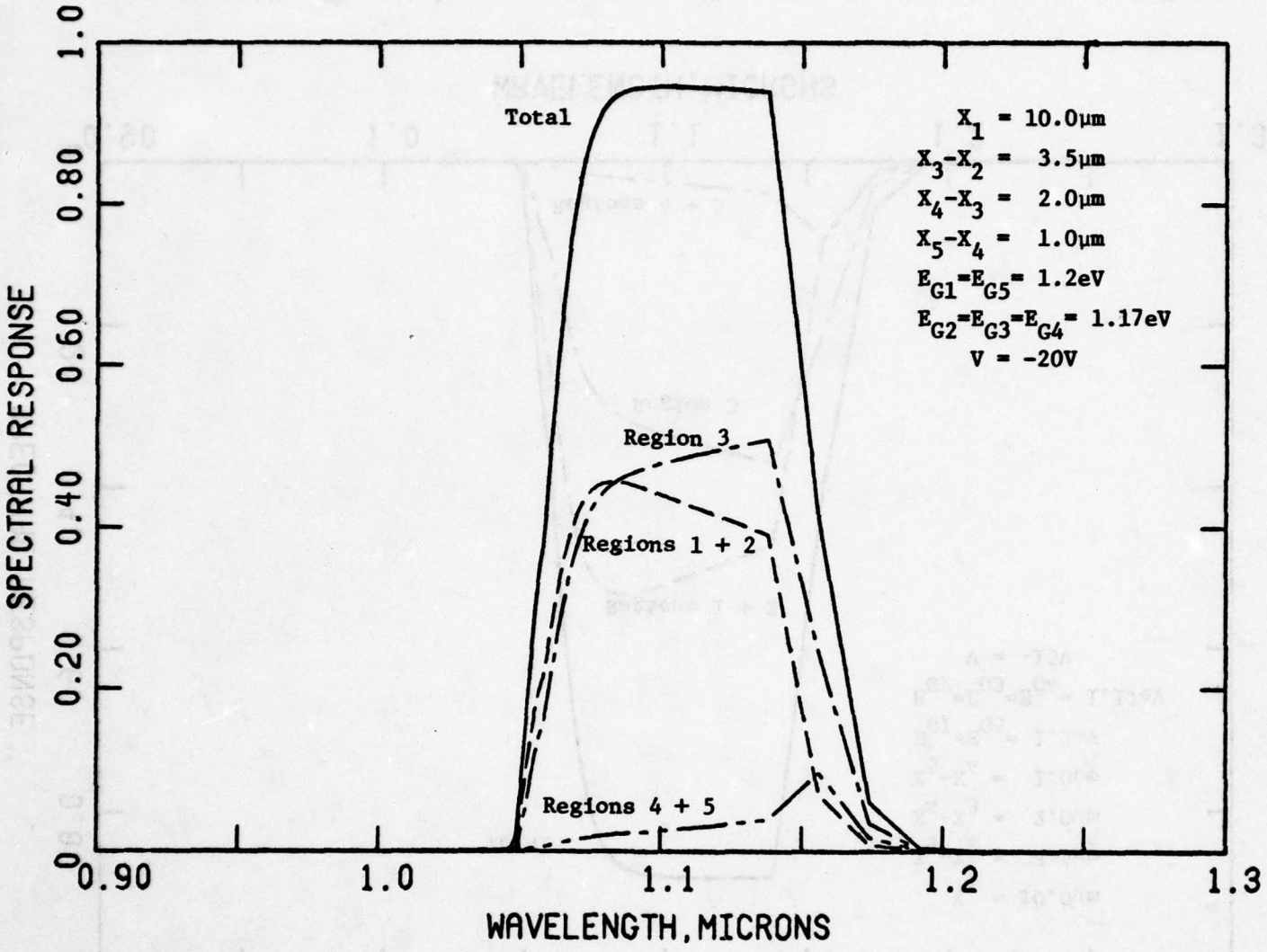

Figure 6(c). Photodiode spectral response in non-avalanche mode for V = -20 V.

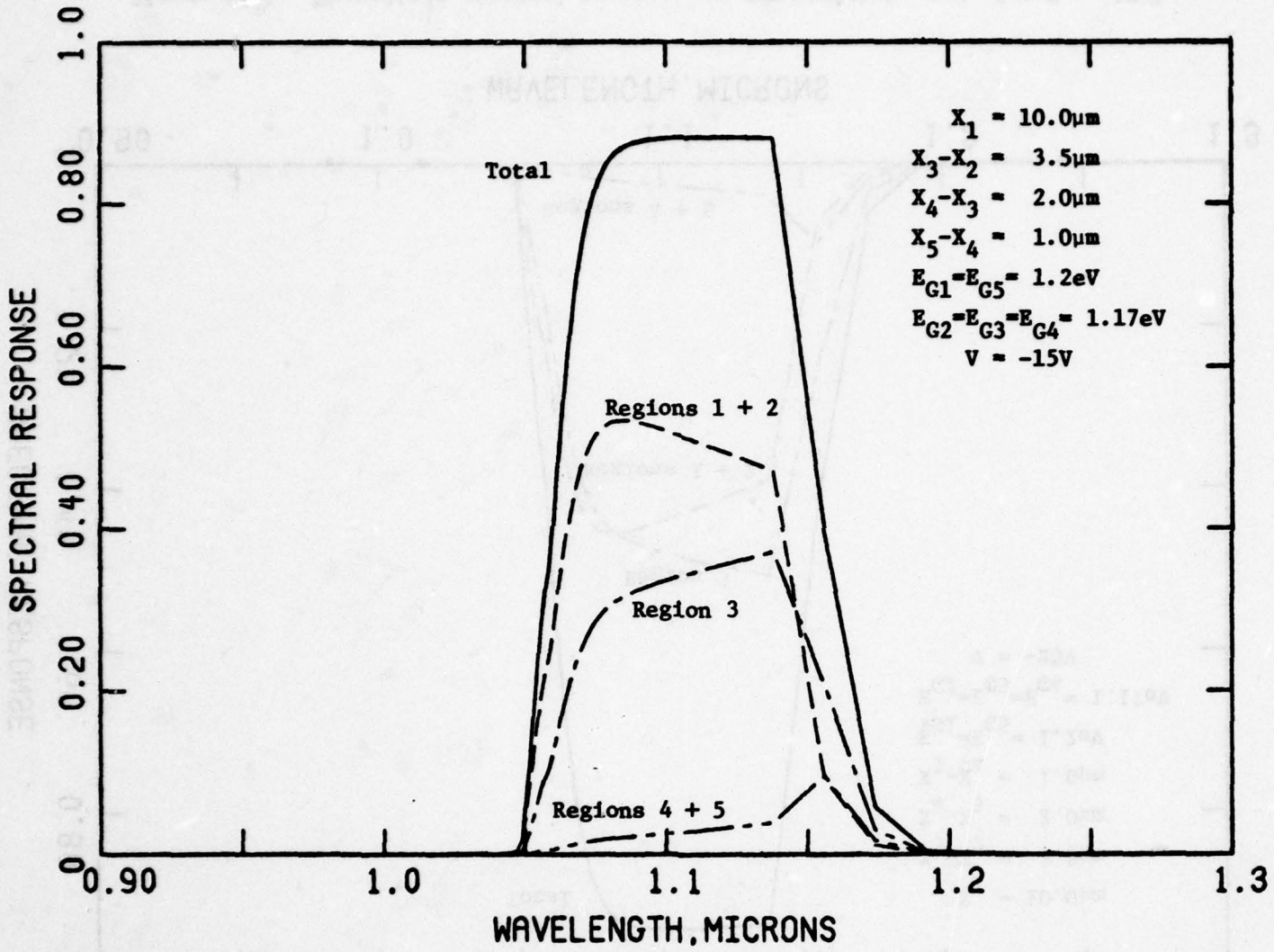

Figure 6(d). Photodiode spectral response in non-avalanche mode for V = -15 V.

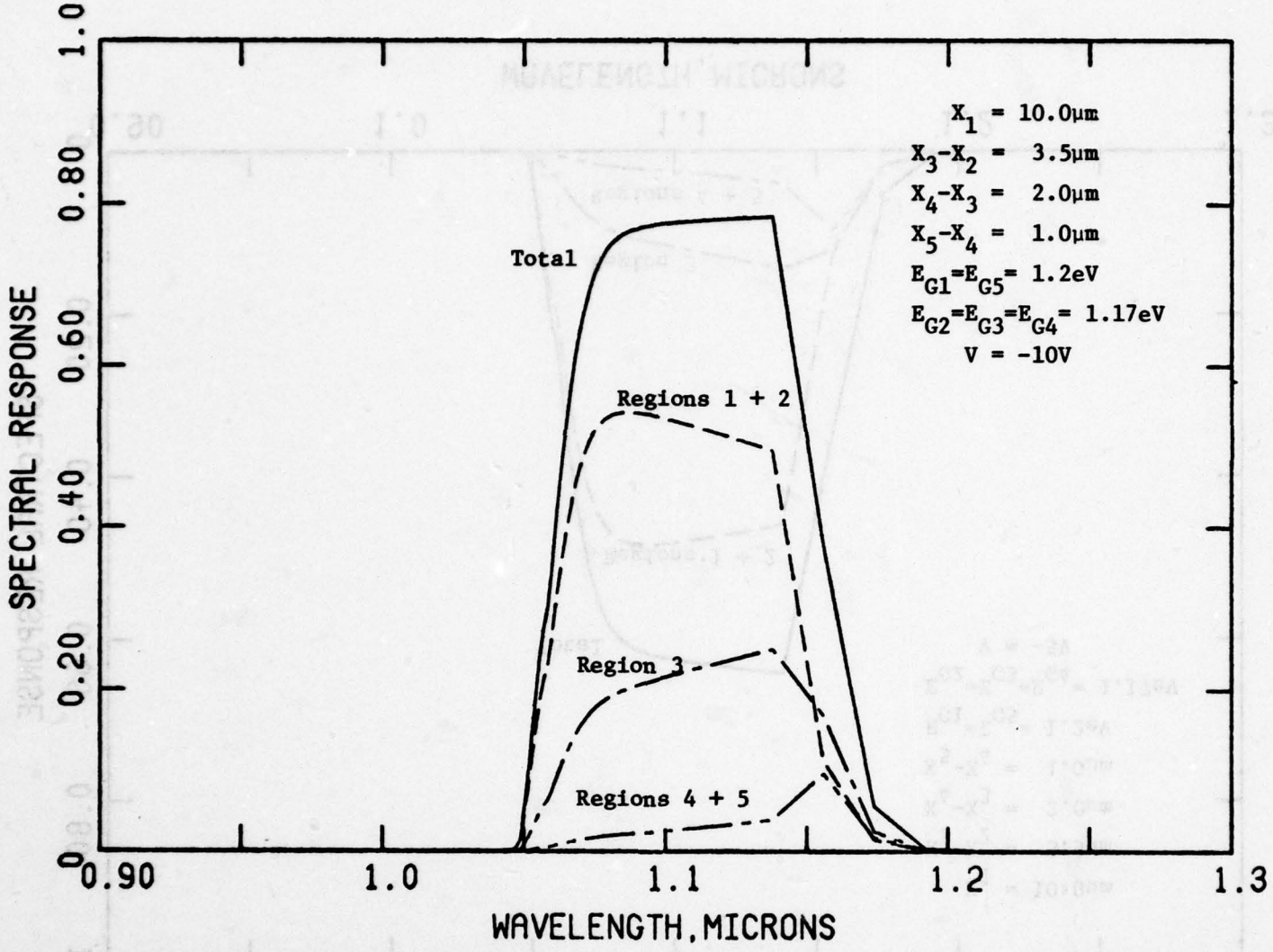

Figure 6(e). Photodiode spectral response in non-avalanche mode for V = -10 V.

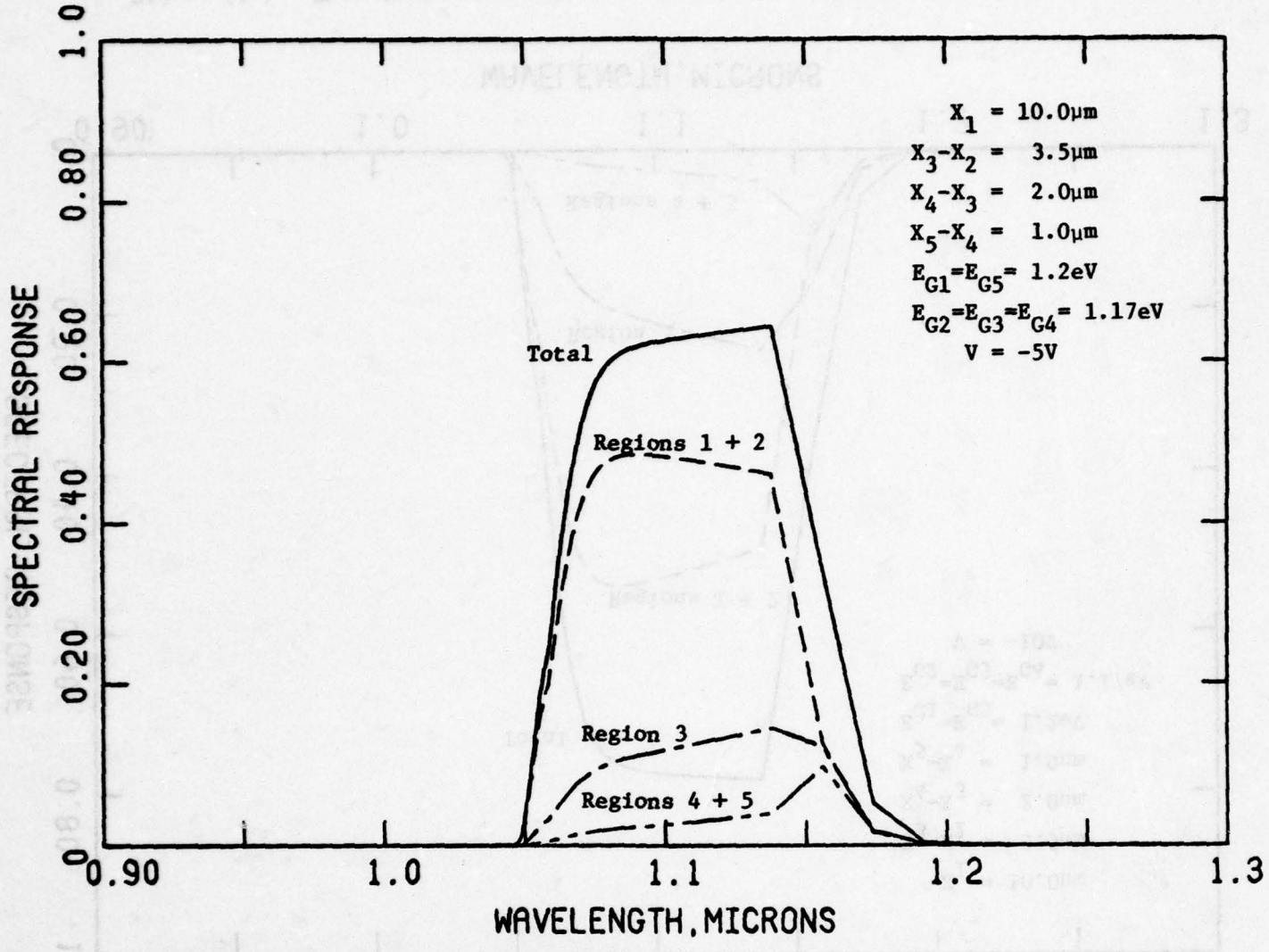

Figure 6(f). Photodiode spectral response in non-avalanche mode for V = -5 V.

To pursue a more direct study of the optimum depletion layer thickness, a set of spectral response curves was calculated in which the depletion layer thickness is changed from 2.0 to 5.0 μm. These results are given in Figures 7(a) through 7(g). The hole contribution to total spectral response in Regions 1 and 2 is unchanging because the materials and their thicknesses are held constant. Due to the change of the depleted region layer thickness, the response curves of Region 3 and Regions 4 and 5 do change with increasing depleted layer thickness. With increasing depleted layer thickness, the hole response in Region 3 increases while the electron response in Regions 4 and 5 decreases. This arises because of increased absorption in Region 3 which in turn results in a lower photon flux entering Regions 4 and 5. While the hole contribution to spectral response in Region 3 and the total response increase significantly from 1.99 to 3.49 μm, the rate of increase beyond 3.49 μm is not great. This substantiates our conclusion that 3.5 μm is in the neighborhood of the optimum thickness for the depleted region.

The influence of the bandgap in Regions 1 and 5 on spectral response and dark current was also investigated. In order to perform these calculations, it is necessary to calculate the hole and electron mobility in Regions 1 and 5, respectively, because experimentally determined values are generally not available for the range of ternary alloy compositions studied. The mobilities are calculated by extrapolation from the mobility values of the terminal binary alloys which comprise the ternaries. The calculated mobility values are approximately 60% higher than the values calculated from the Rockwell International experimentally determined diffusion lengths.

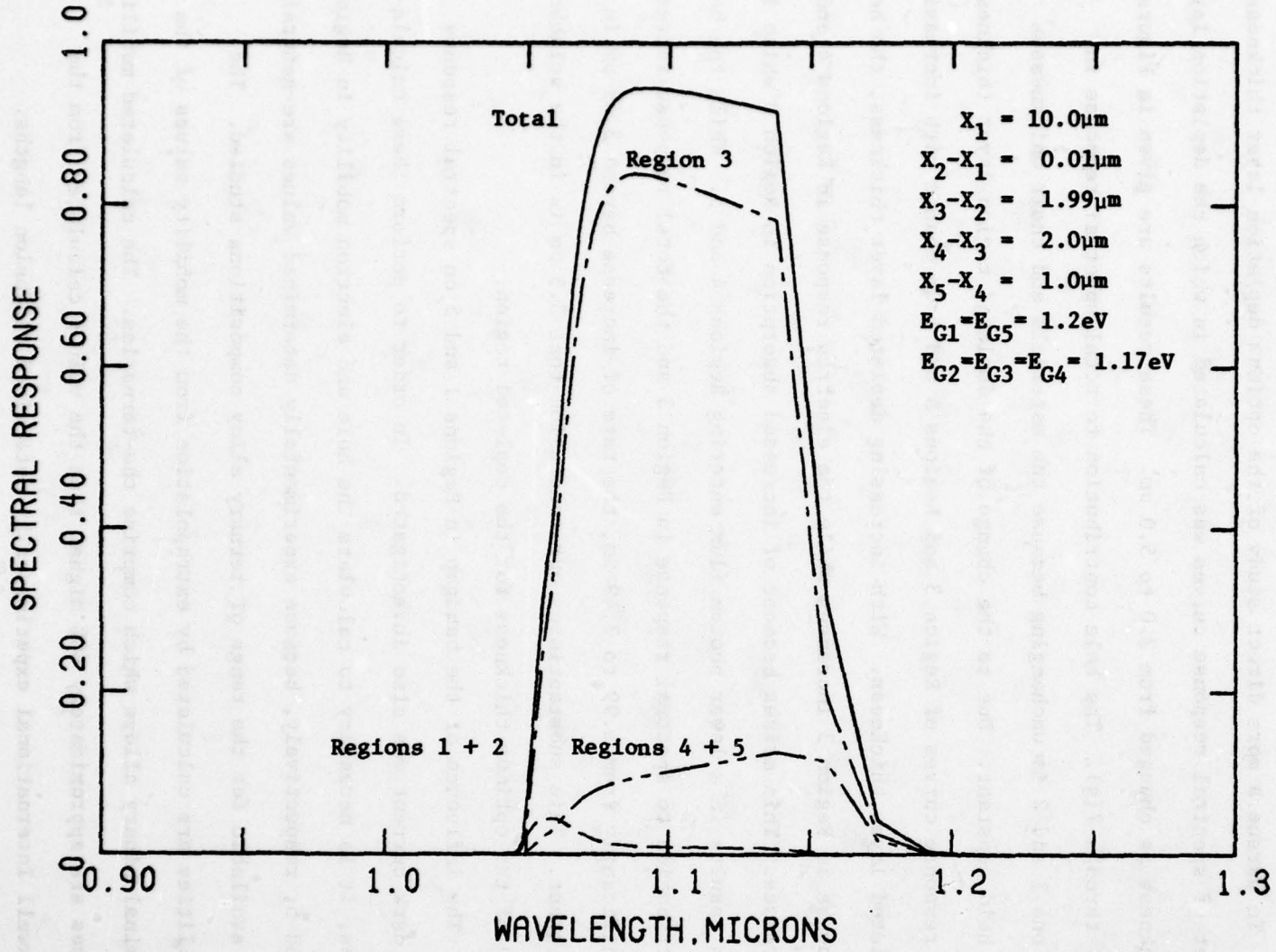

Figure 7(a). Photodiode spectral response in non-avalanche mode for 1.99 μm depletion layer thickness.

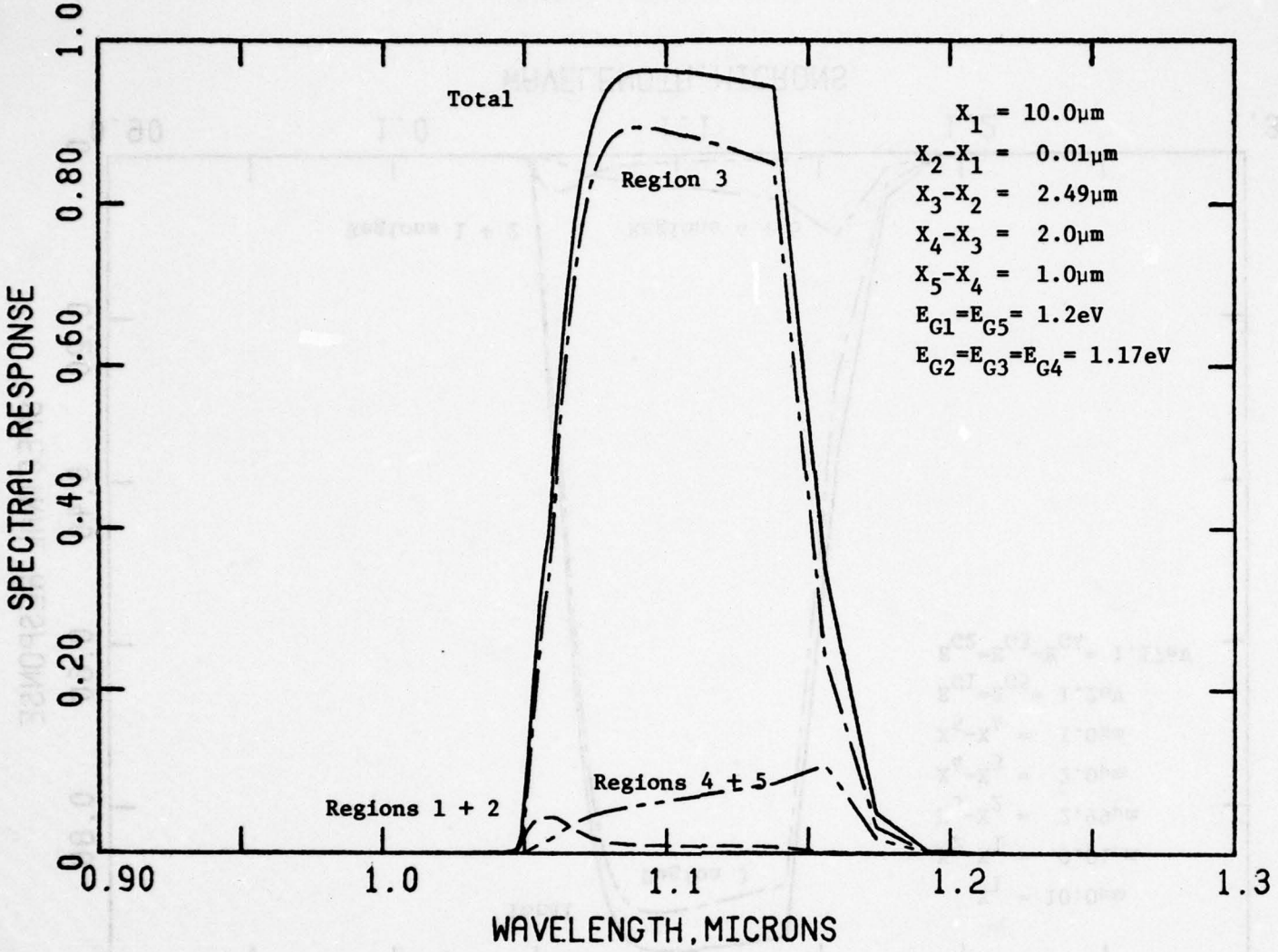

Figure 7(b). Photodiode spectral response in non-avalanche mode for 2.49 μm depletion layer thickness.

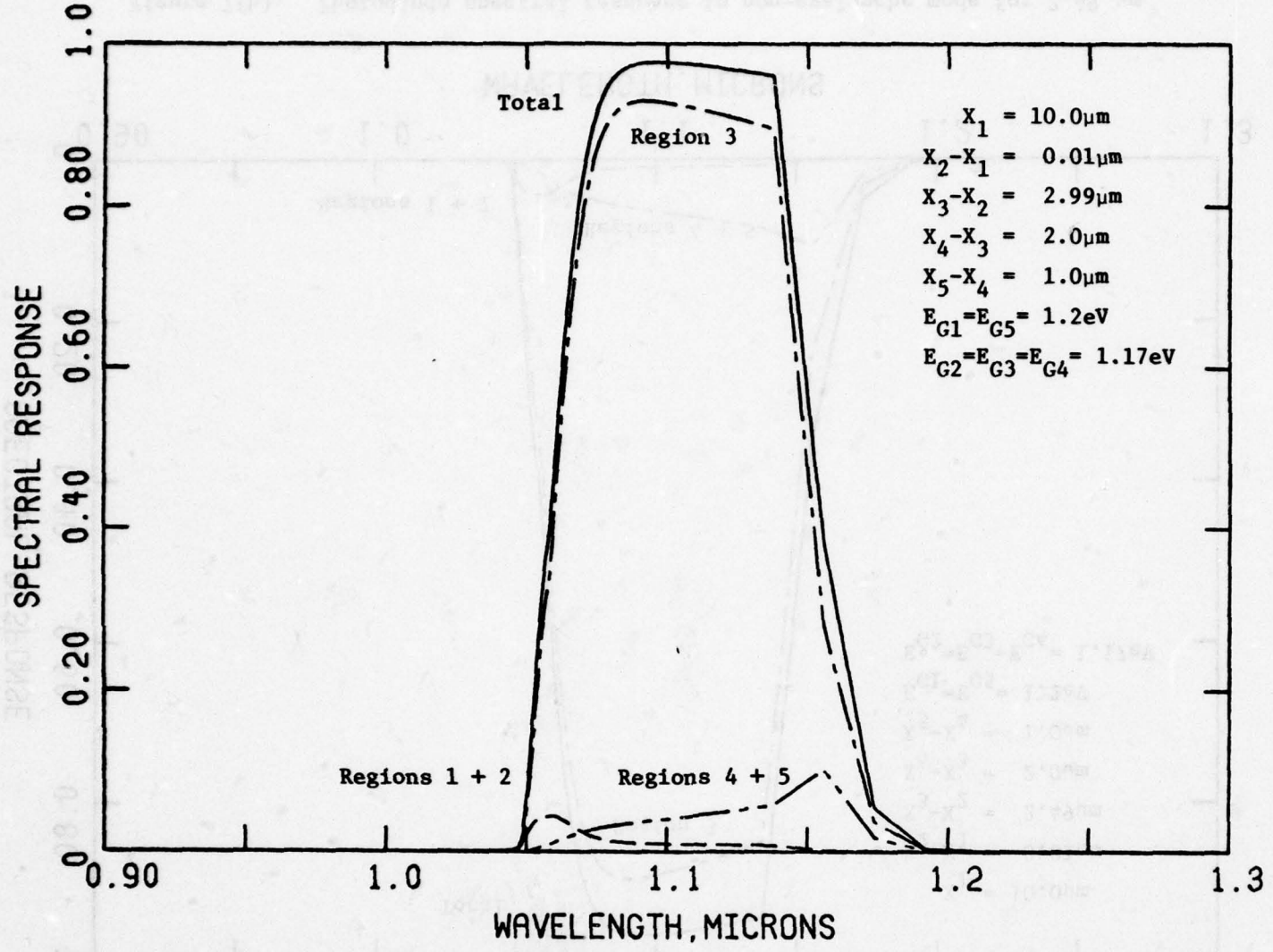

Figure 7(c). Photodiode spectral response in non-avalanche mode for 2.99 μm depletion layer thickness.

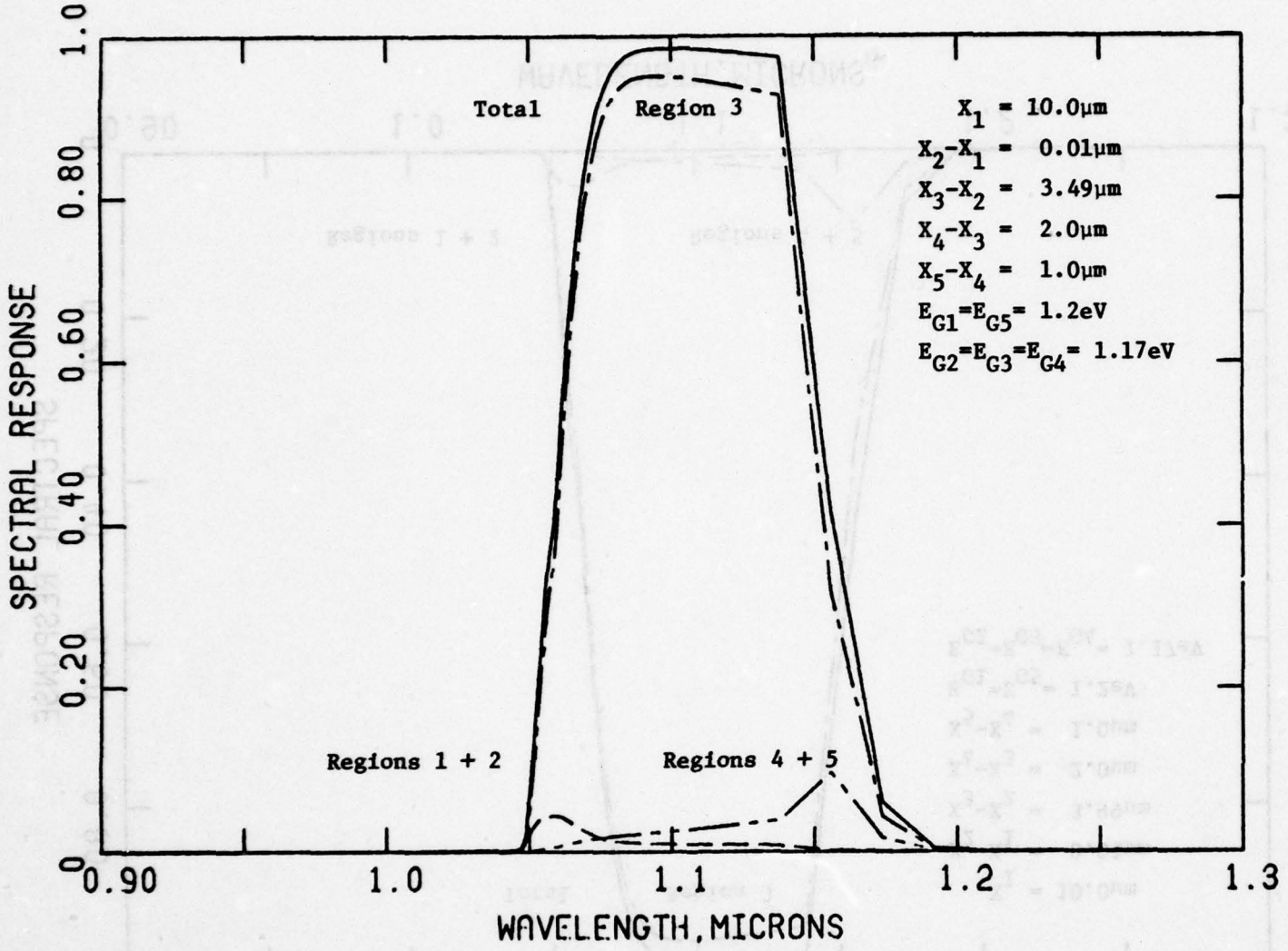

Figure 7(d). Photodiode spectral response in non-avalanche mode for 3.49 μm depletion layer thickness.

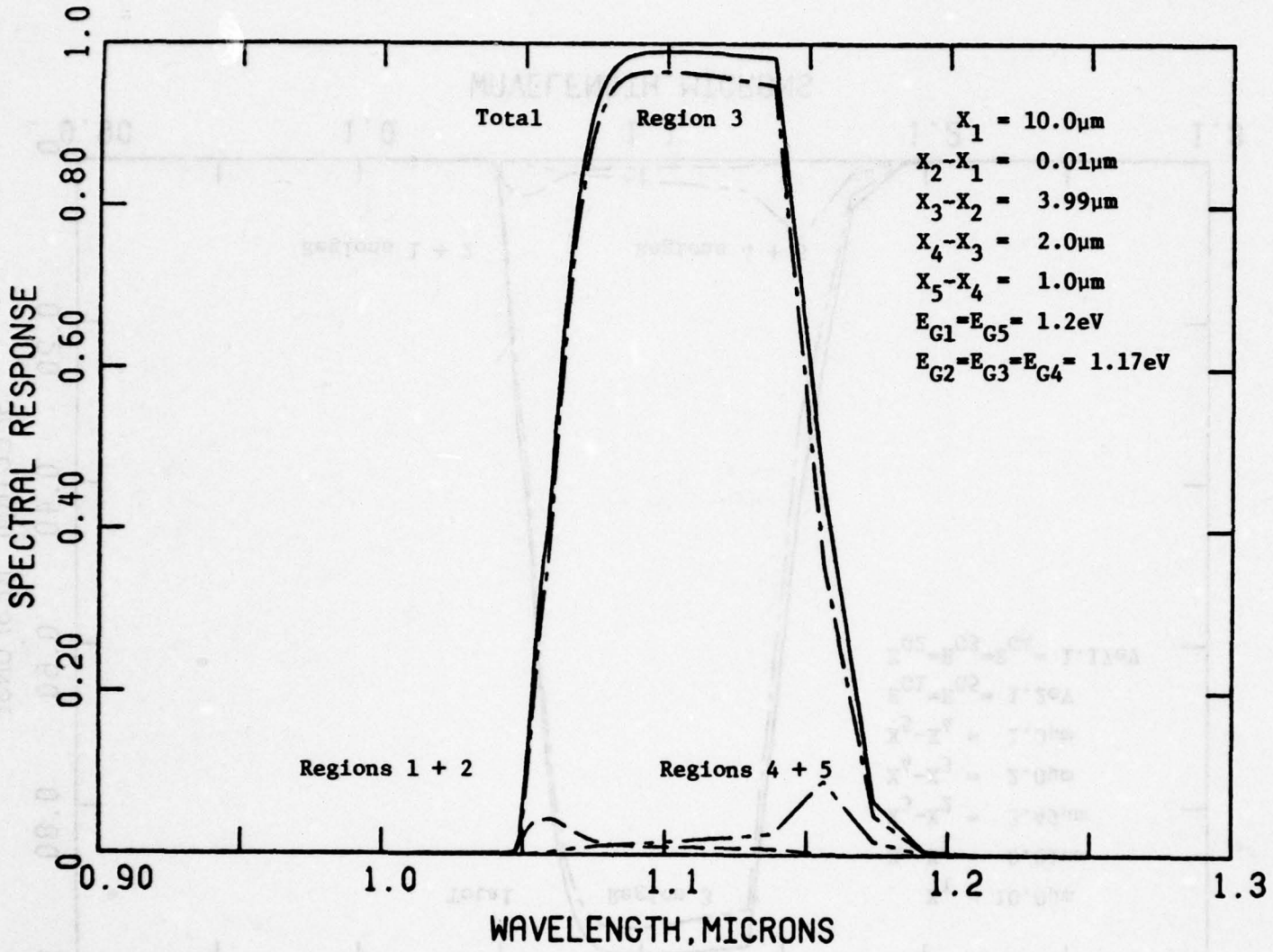

Figure 7(e). Photodiode spectral response in non-avalanche mode for 3.99 μm depletion layer thickness.

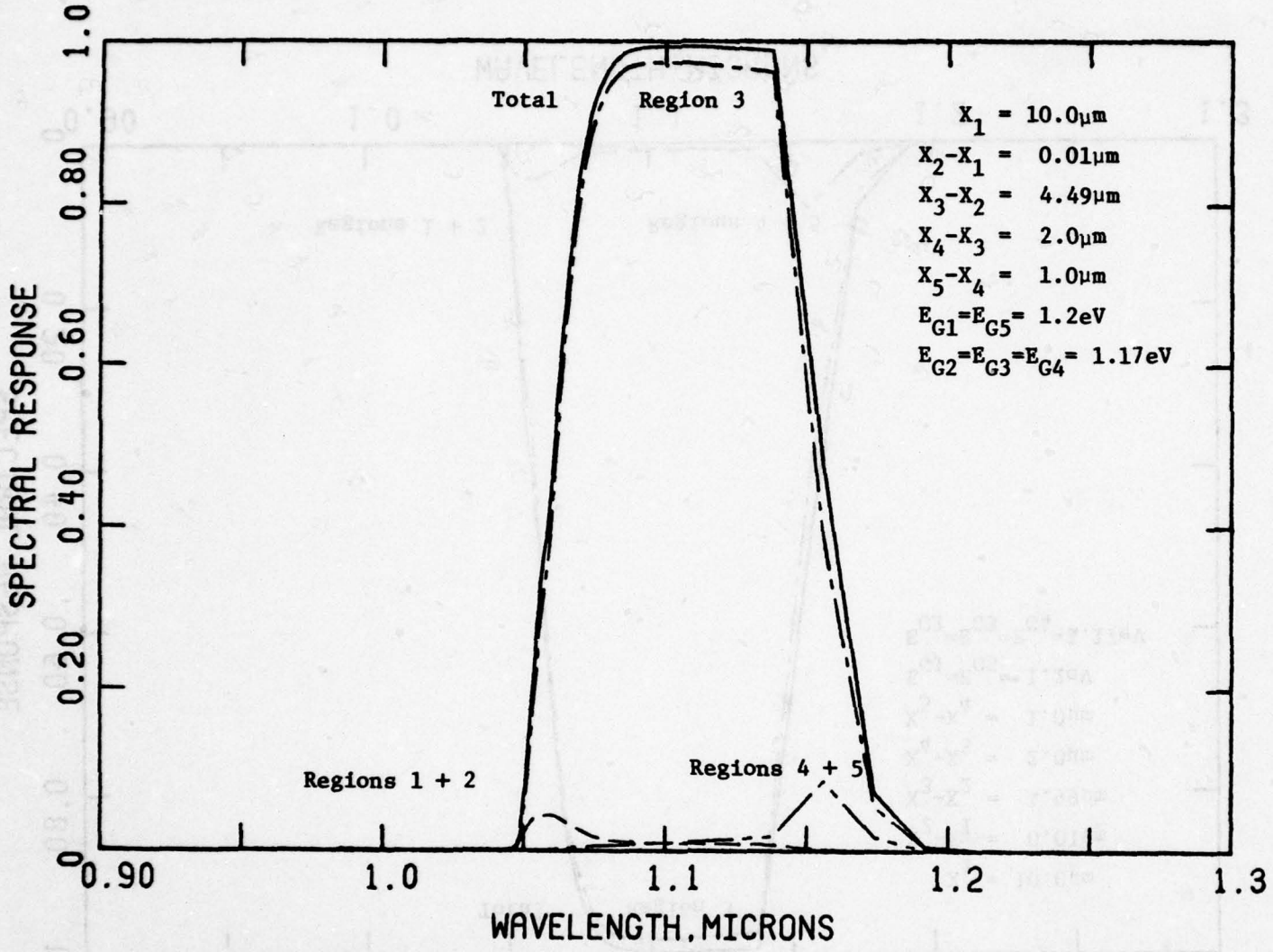

Figure 7(f). Photodiode spectral response in non-avalanche mode for 4.49 μm depletion layer thickness.

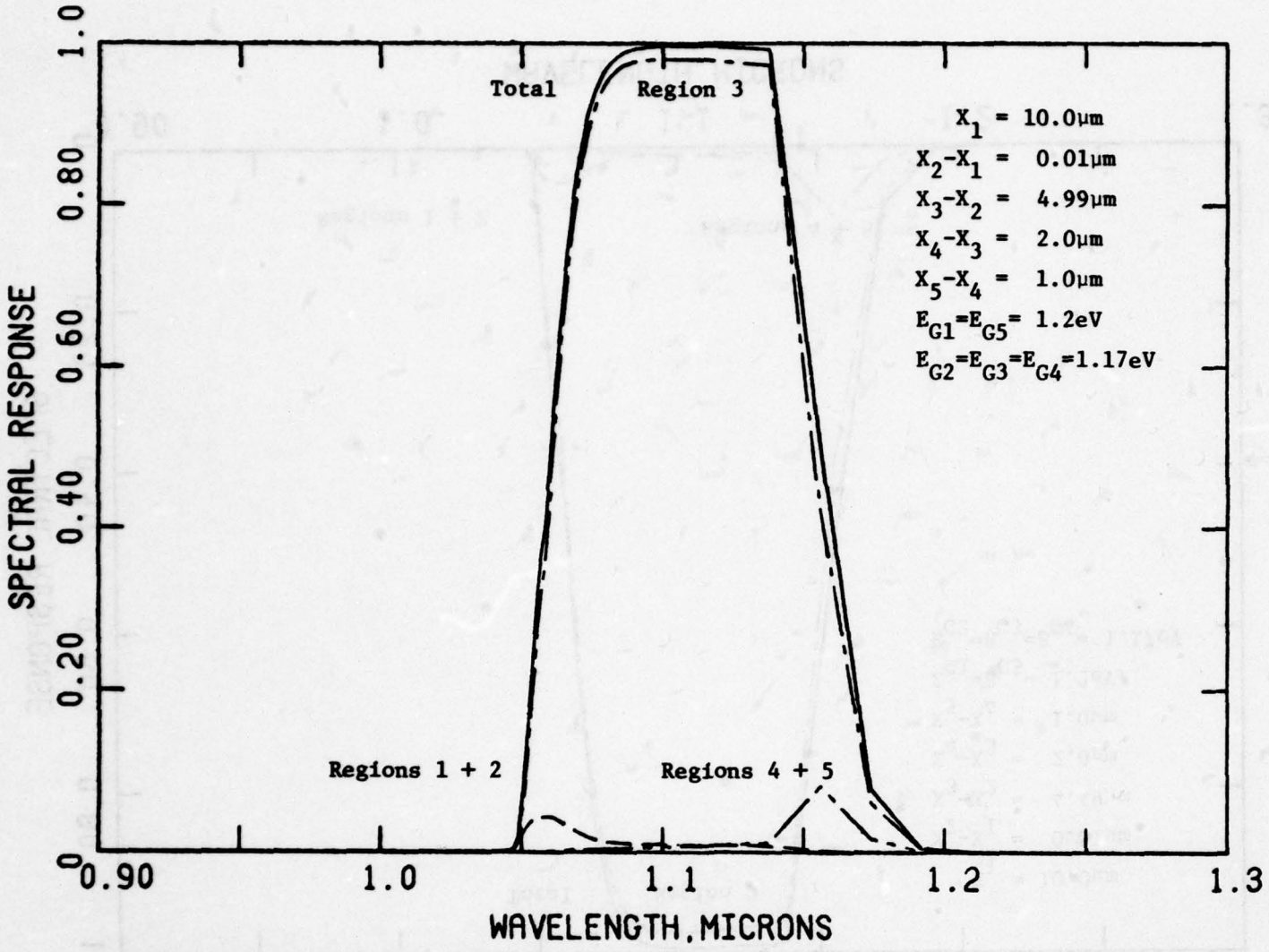

Figure 7(g). Photodiode spectral response in non-avalanche mode for 4.99 μm depletion layer thickness.

The spectral responses, where Region 1 and 5 bandgaps are a parameter, are shown in Figures 8(a) through 8(h). The bandgap ranges from 1.16 to 1.30 eV. These curves show that the hole contribution to spectral response in Regions 1 and 2 is significantly higher than previous calculations for X_1=10 μm for all bandgap values. The major reason for this is that the calculated mobility is higher than the experimentally determined value. The response in Regions 1 and 2 decreases slightly with increasing bandgap. This is attributed to less absorption which results with increasing bandgap.

The short wavelength cut-off shifts to shorter wavelengths with increasing bandgap. As a result, the spectral response in Region 3 shifts to shorter wavelength since the photon flux entering Region 3 increases.

For completeness, the final study conducted was to determine the optimum thickness of the p^+ layer, Region 4. The layer thickness range studied was from 0.2 to 2.0 μm, maintaining constant bandgap at 1.2 eV. These calculations in Figures 9(a) to 9(f) show that the electron contribution to spectral response increases in Regions 4 and 5 with increasing layer thickness. For highest S/N, the spectral response in Regions 4 and 5 should be as small as possible. While the contribution to spectral response from Regions 4 and 5 is small for Region 4 thicknesses of 0.2 and 0.4 μm, it increases only slightly up to 0.8 μm. Further work is required to determine the optimum Region 4 thickness. However, we may tentatively conclude that Region 4 thickness should be less than 1.0 μm.

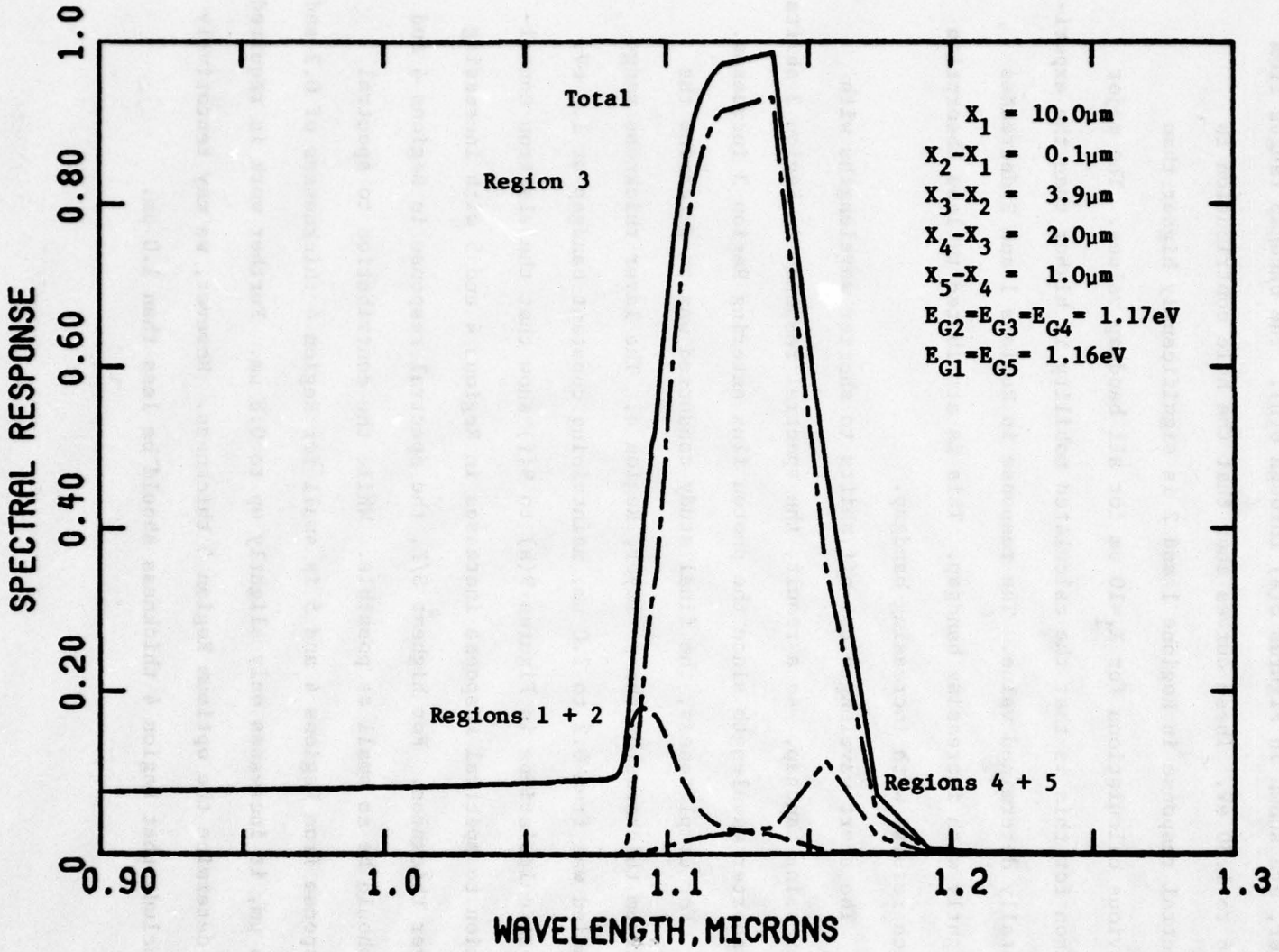

Figure 8(a). Photodiode spectral response in non-avalanche mode for bandgap values of 1.16 eV for E_{G1} and E_{G5}.

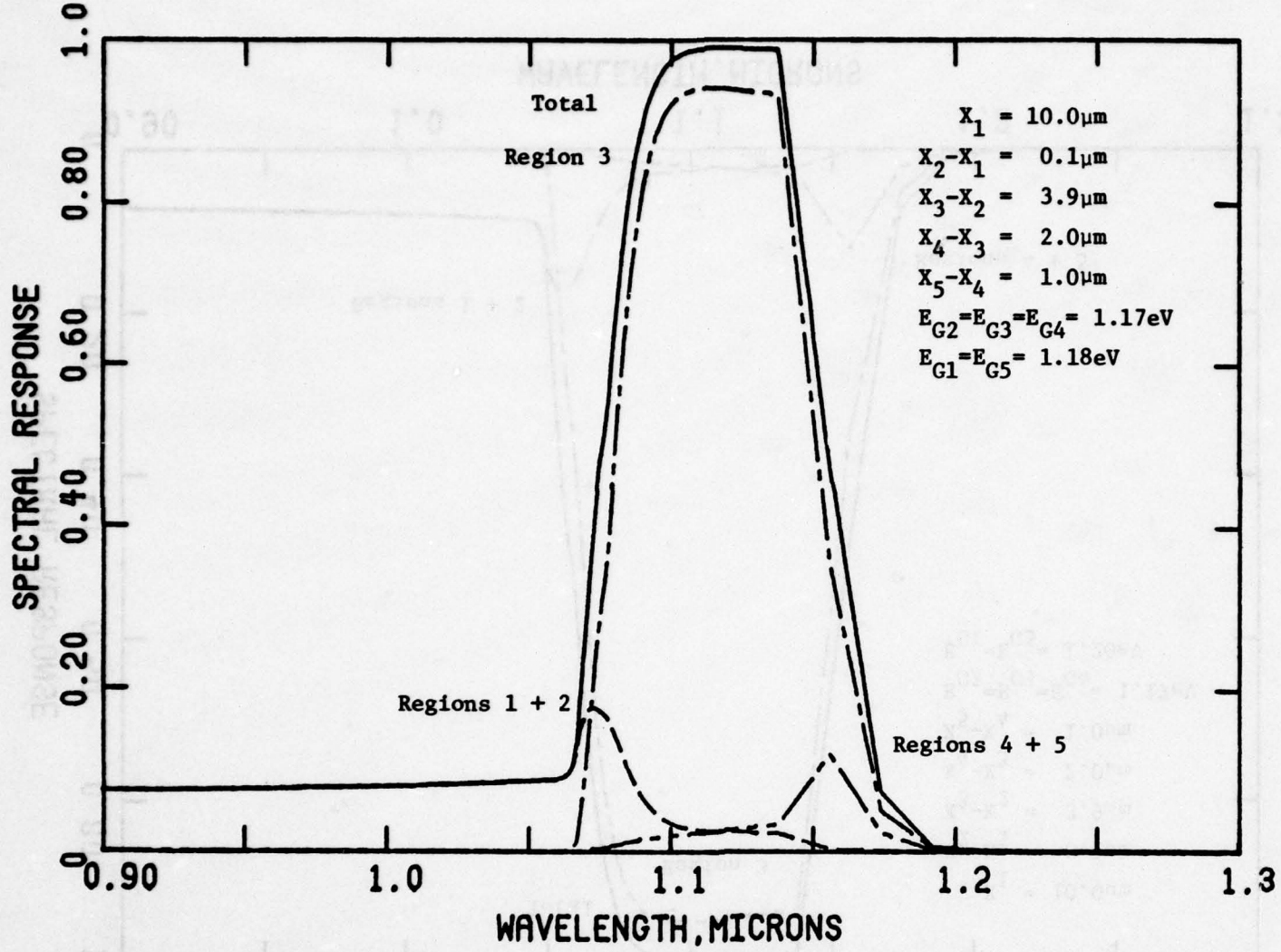

Figure 8(b). Photodiode spectral response in non-avalanche mode for bandgap values of 1.18 eV for E_{G1} and E_{G5}.

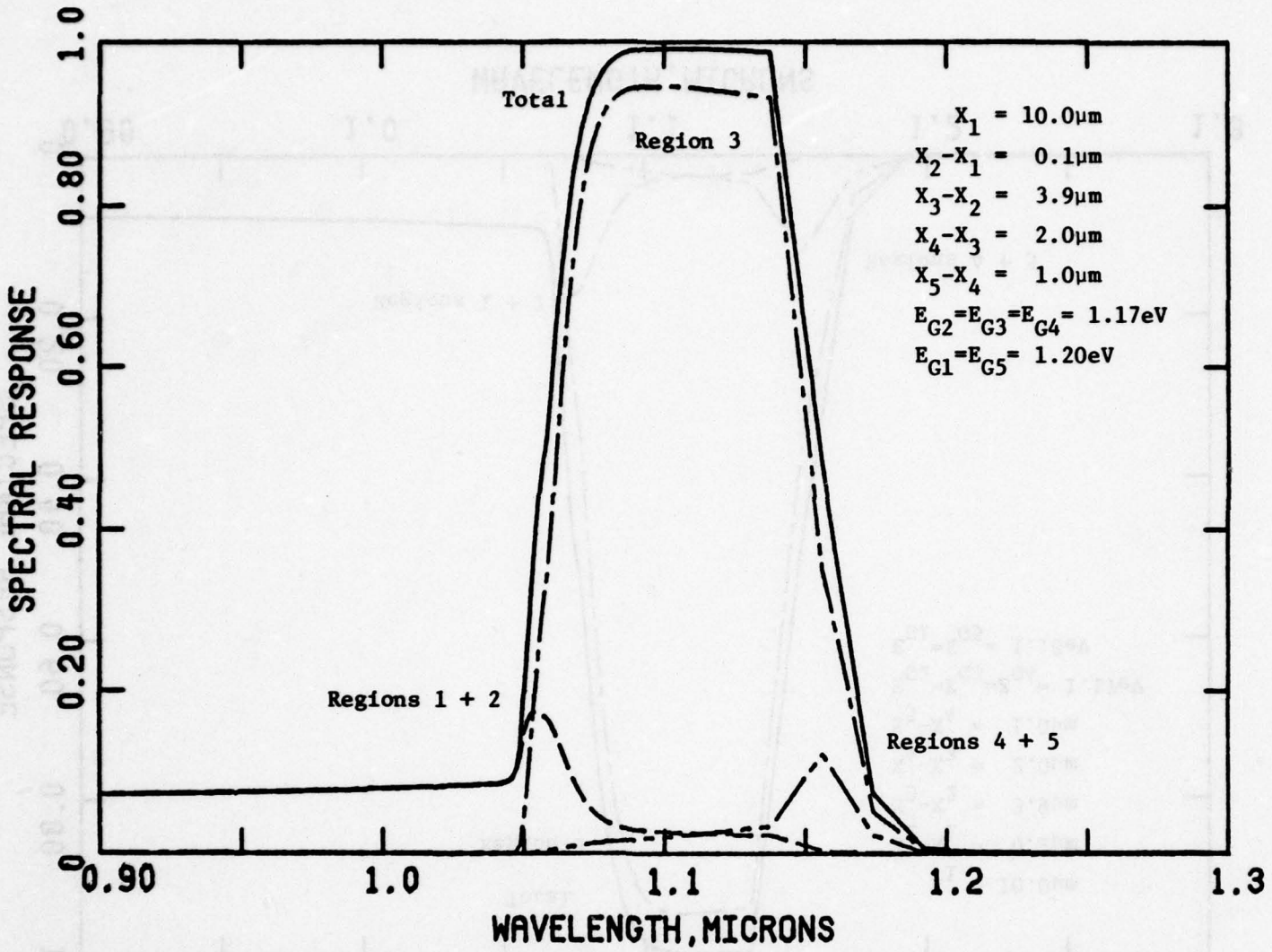

Figure 8(c). Photodiode spectral response in non-avalanche mode for bandgap values of 1.20 eV for E_{G1} and E_{G5}.

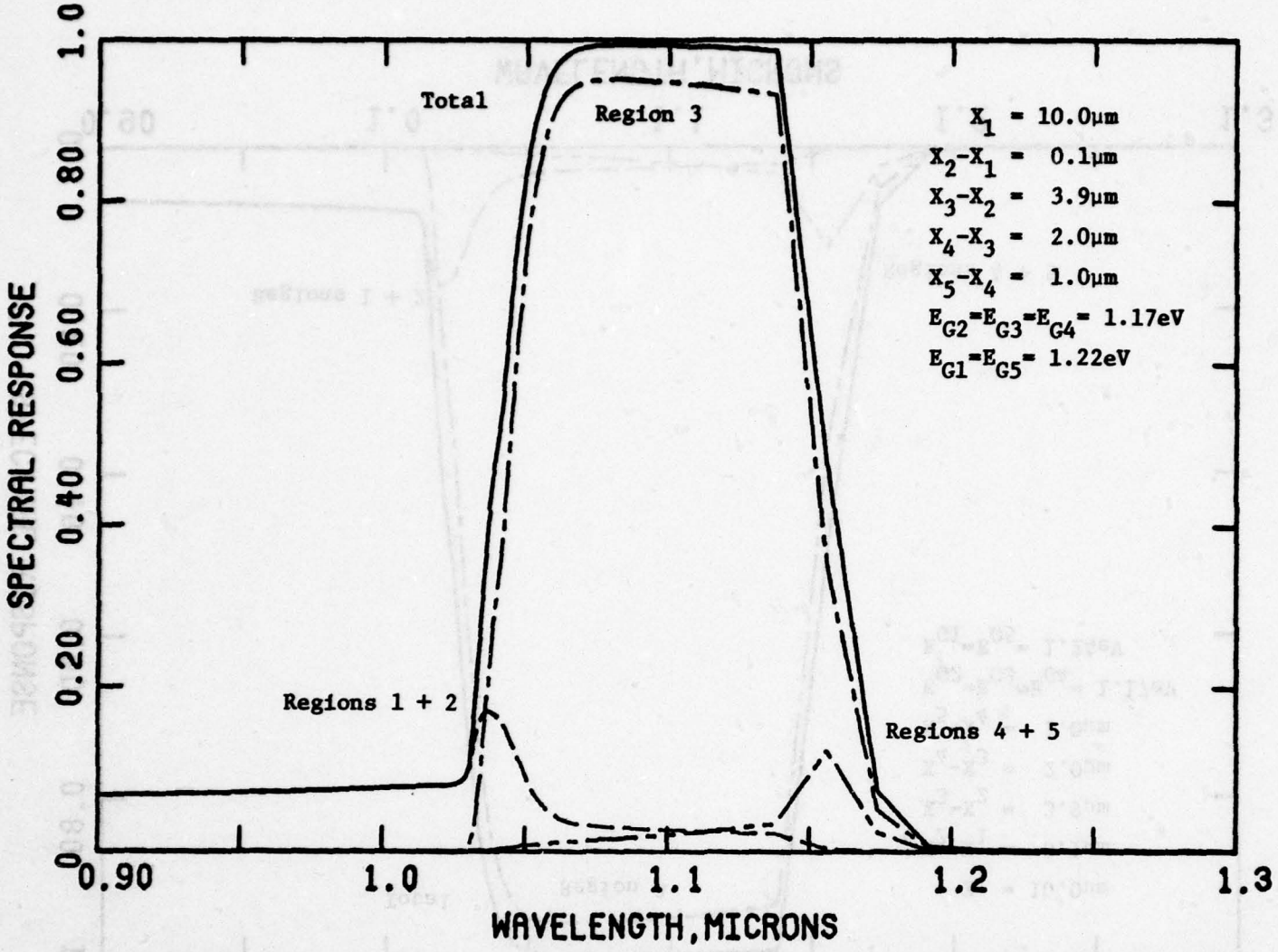

Figure 8(d). Photodiode spectral response in non-avalanche mode for bandgap values of 1.22 eV for E_{G1} and E_{G5}.

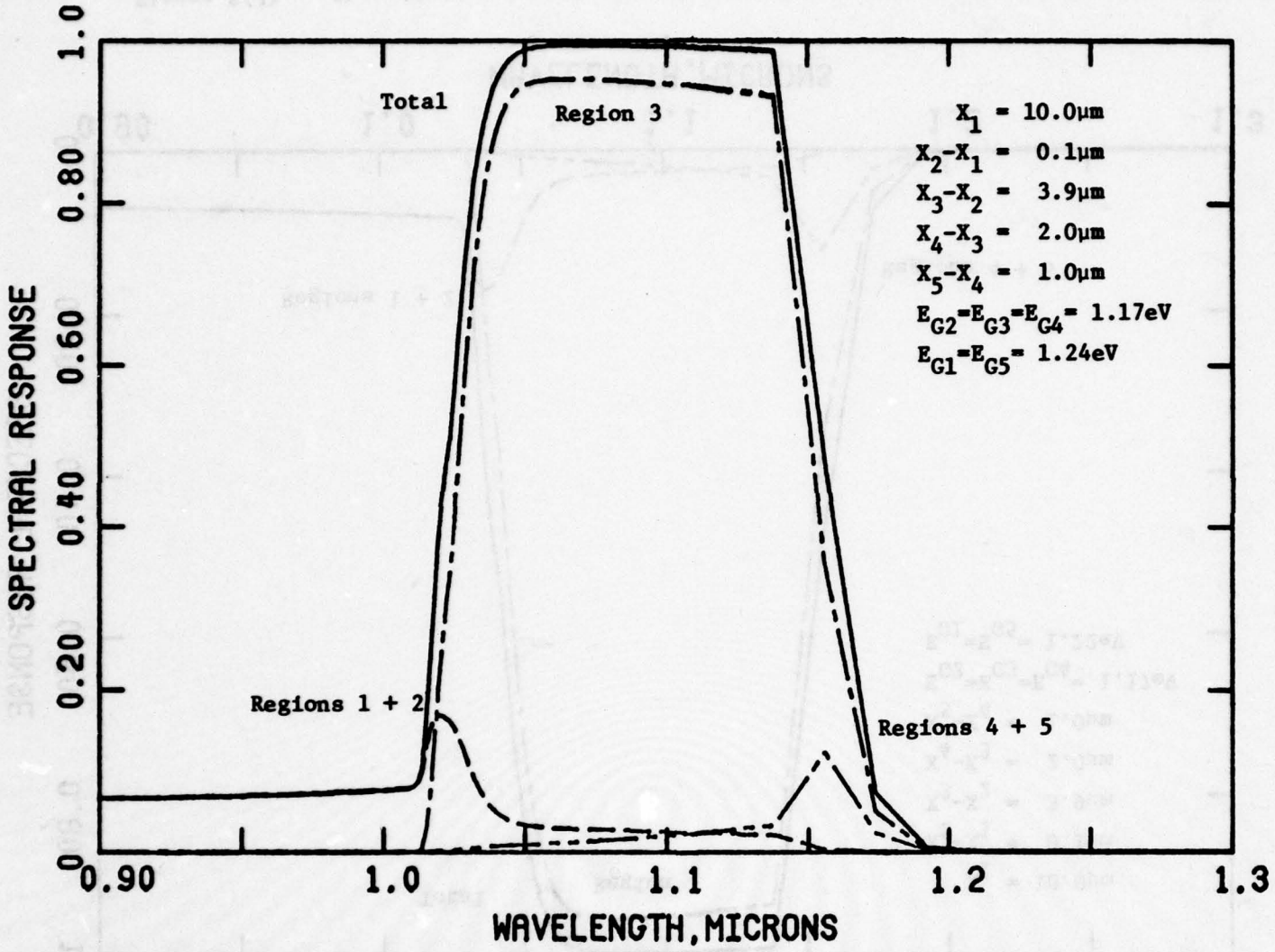

Figure 8(e). Photodiode spectral response in non-avalanche mode for bandgap values of 1.24 eV for E_{G1} and E_{G5}.

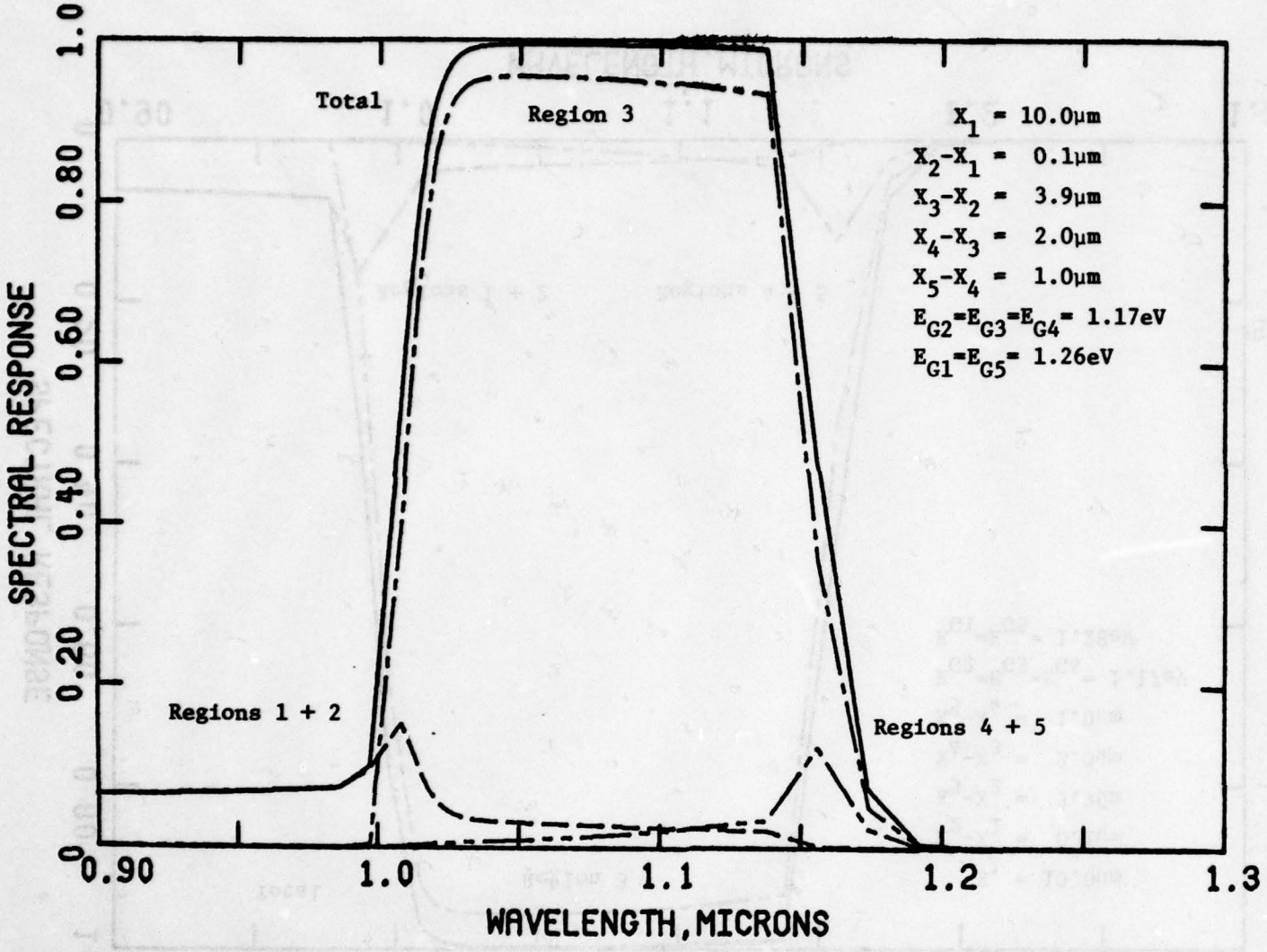

Figure 8(f). Photodiode spectral response in non-avalanche mode for bandgap values of 1.26 eV for E_{G1} and E_{G5}.

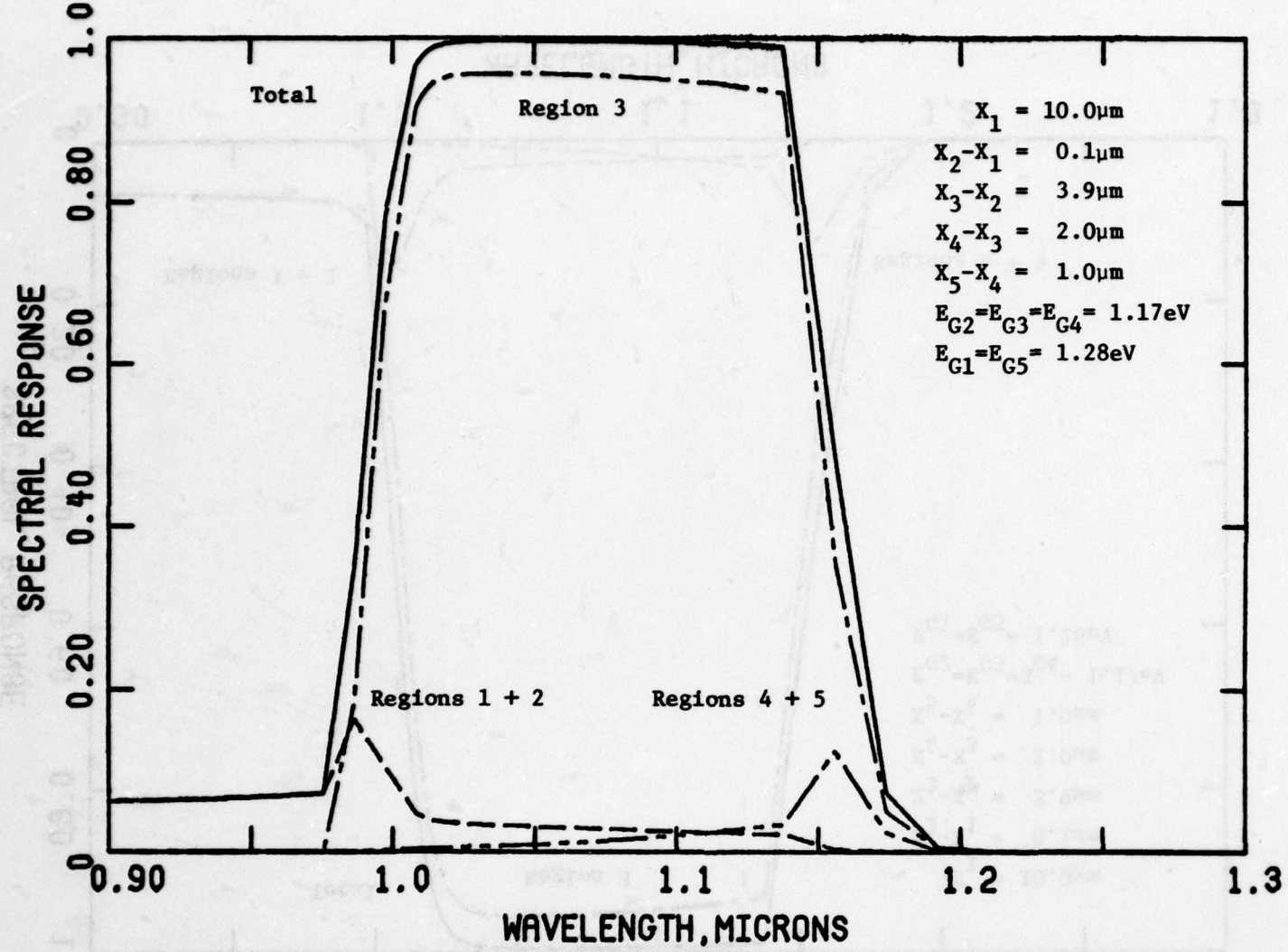

Figure 8(g). Photodiode spectral response in non-avalanche mode for bandgap values of 1.28 eV for E_{G1} and E_{G5}.

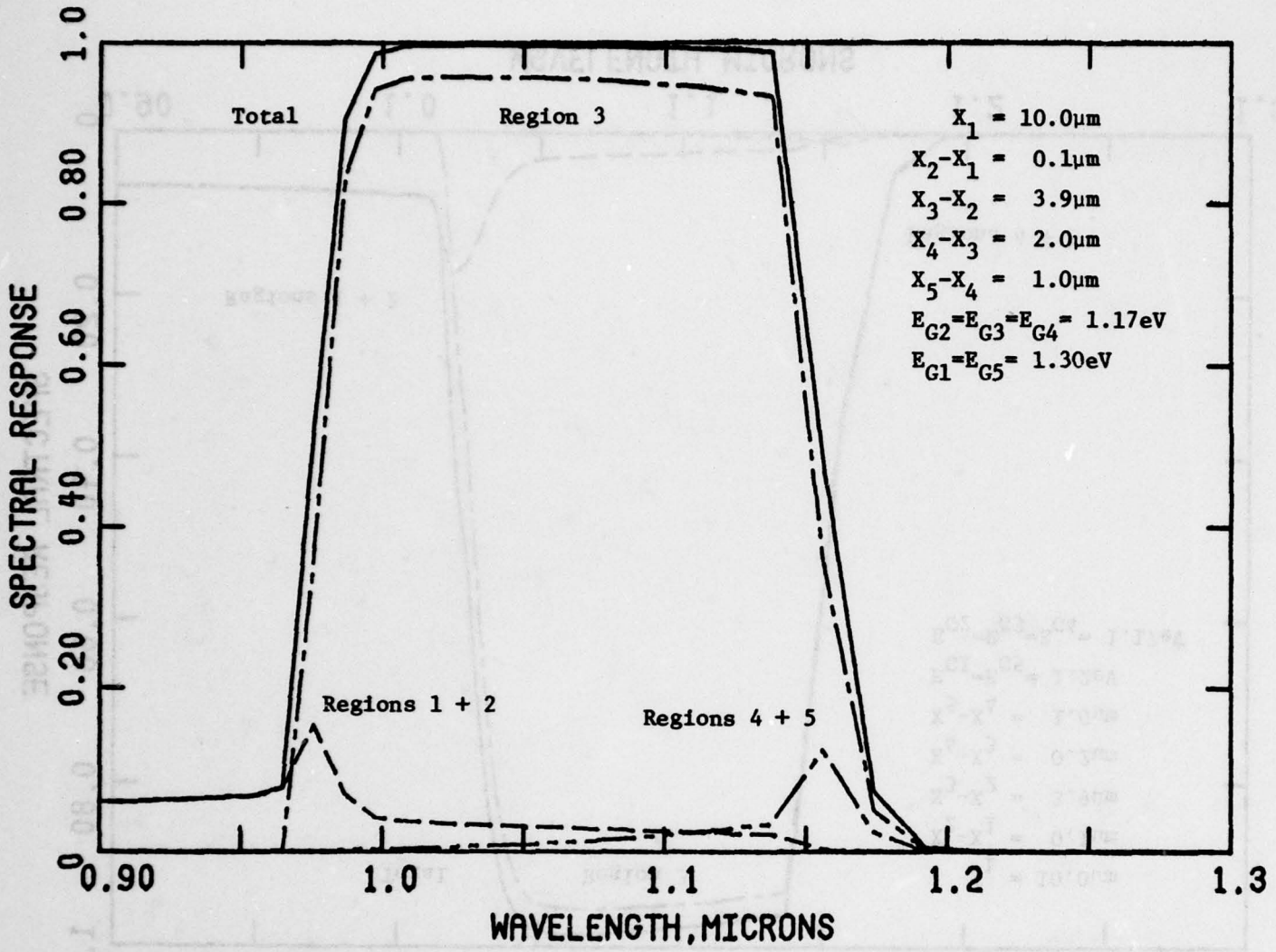

Figure 8(h). Photodiode spectral response in non-avalanche mode for bandgap values of 1.30 eV for E_{G1} and E_{G5}.

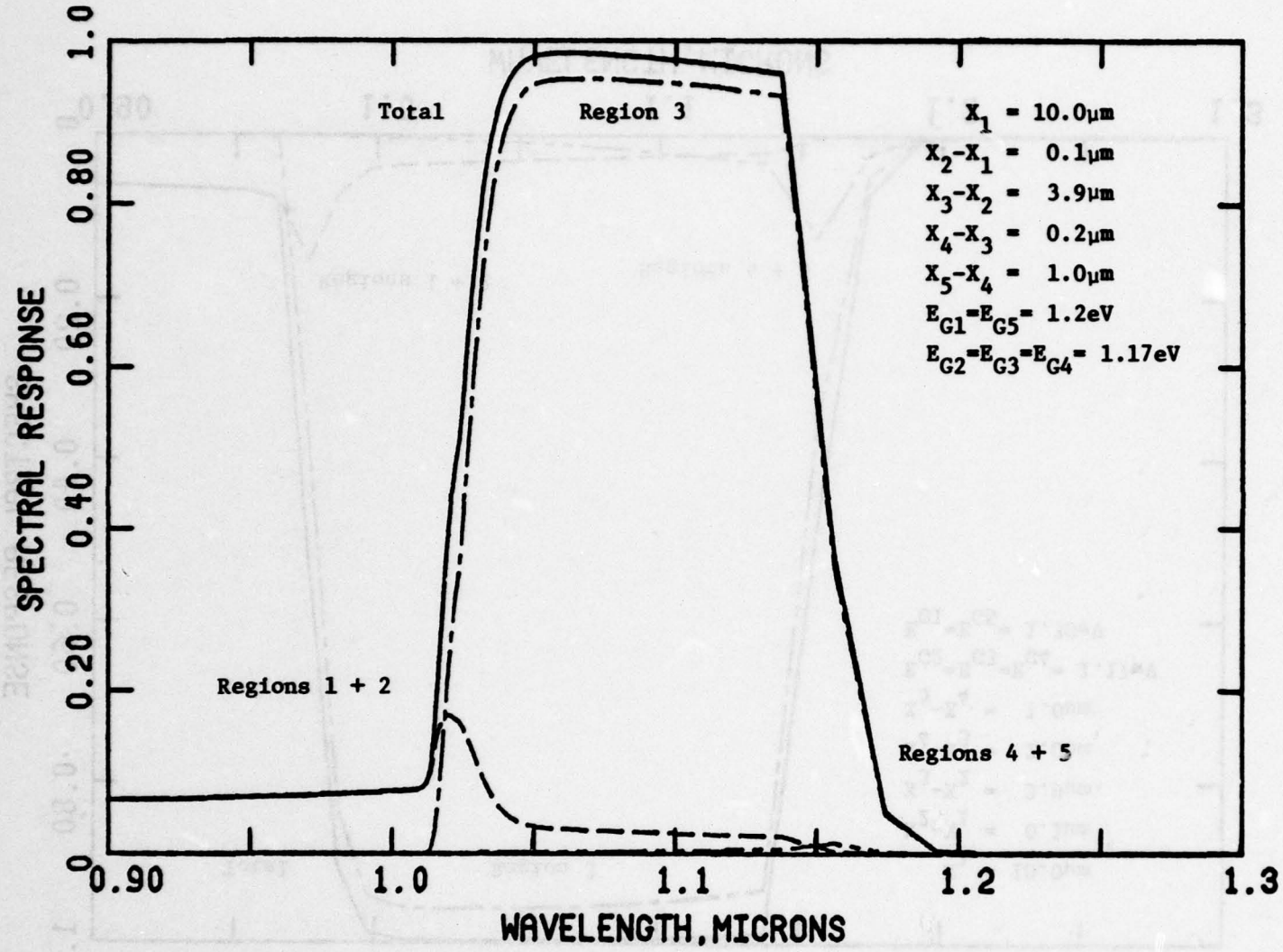

Figure 9(a). Photodiode spectral response in non-avalanche mode for X_4-X_3 = 0.2 μm.

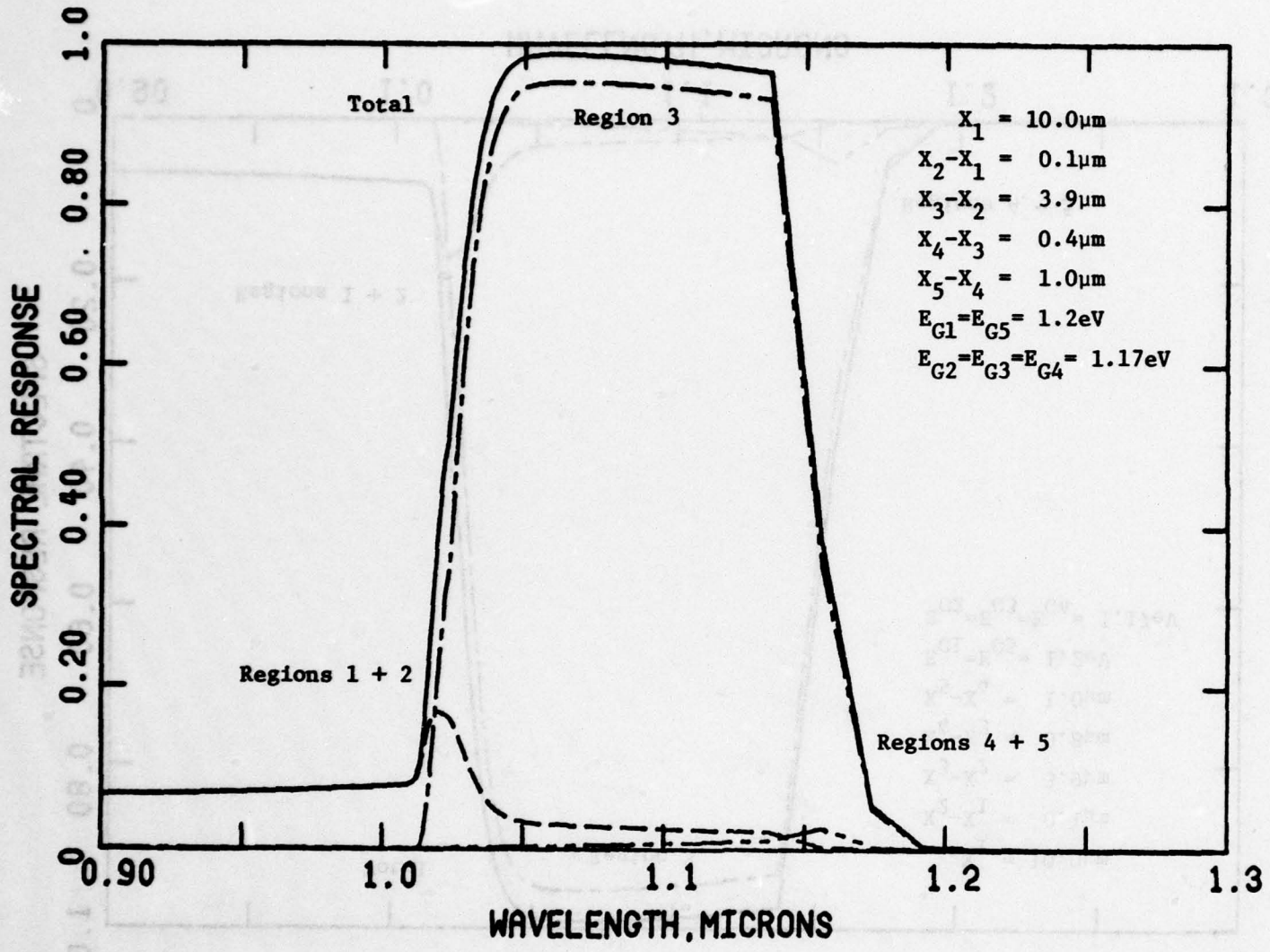

Figure 9(b). Photodiode spectral response in non-avalanche mode for X_4-X_3 = 0.4 μm.

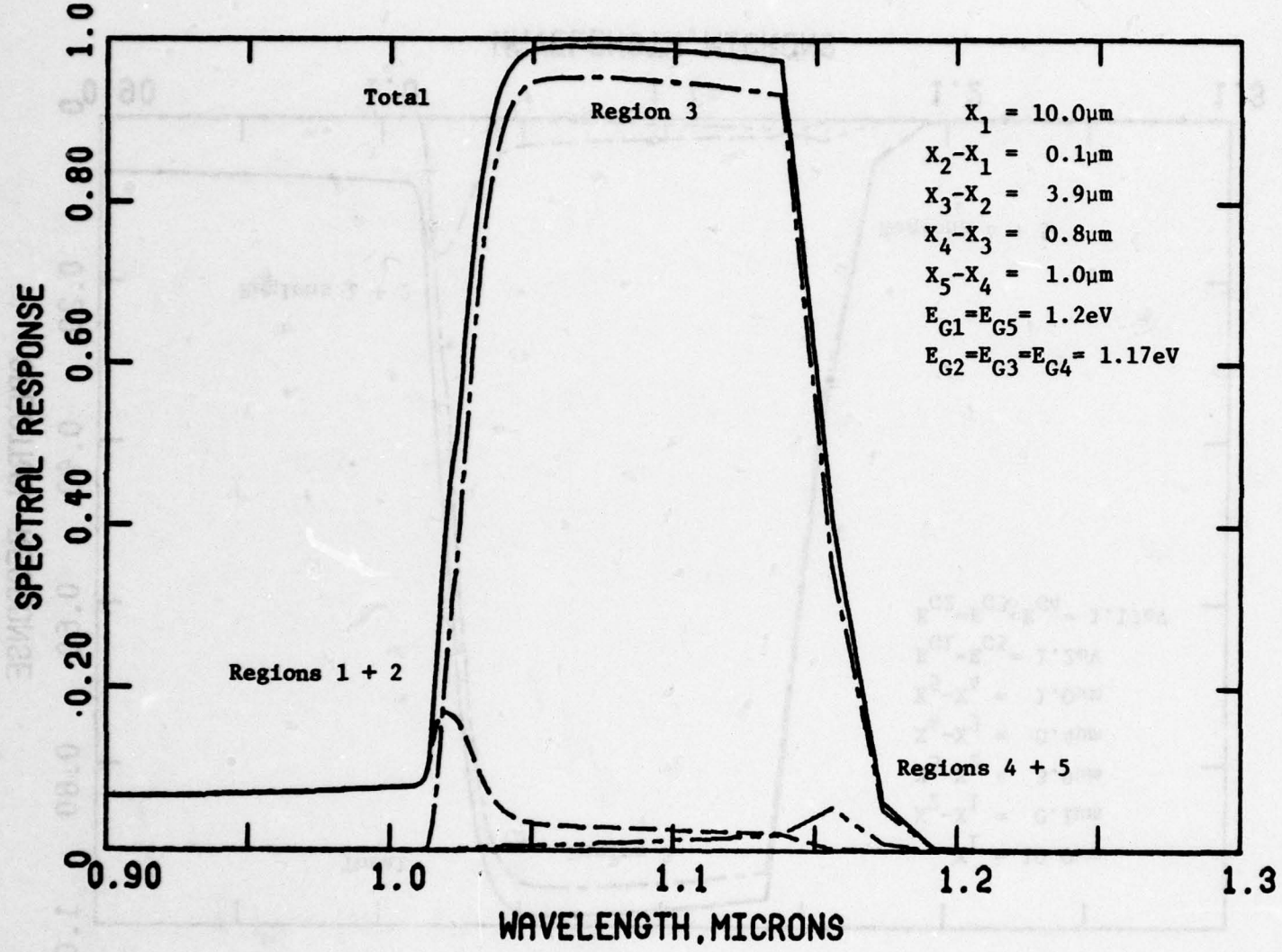

Figure 9(c). Photodiode spectral response in non-avalanche mode for X_4-X_3 = 0.8 μm.

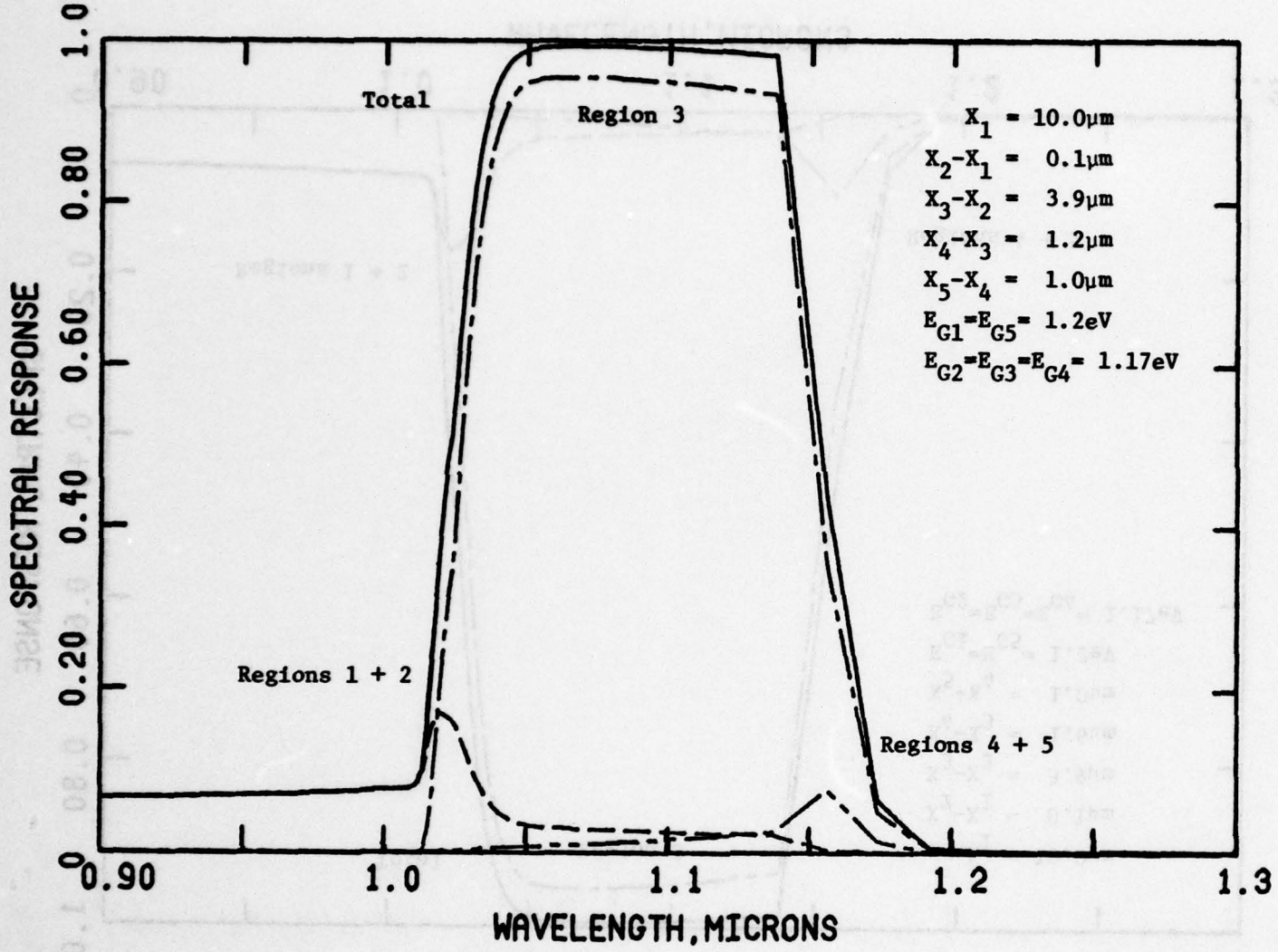

Figure 9(d). Photodiode spectral response in non-avalanche mode for X_4-X_3 = 1.2 μm.

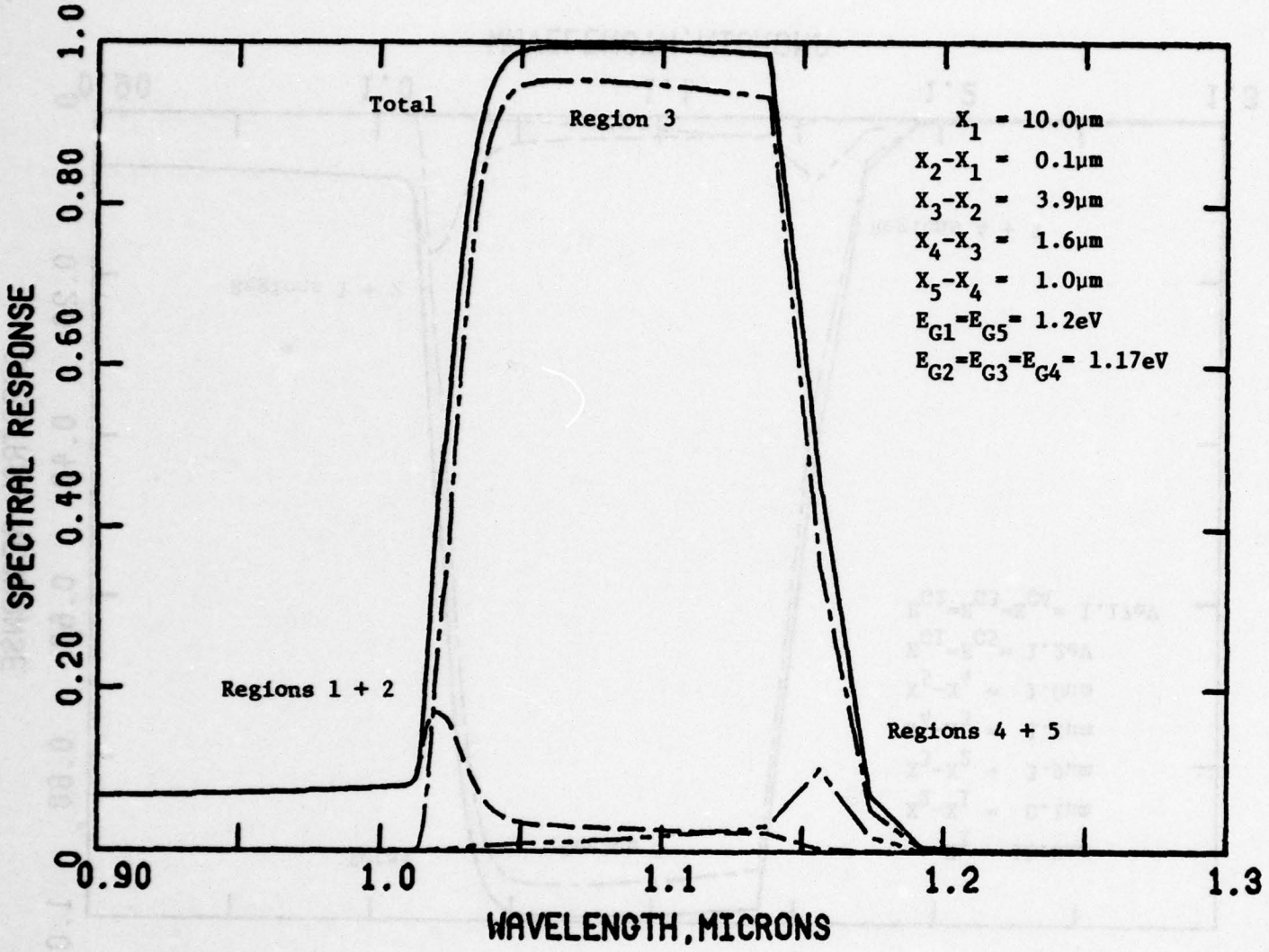

Figure 9(e). Photodiode spectral response in non-avalanche mode for X_4-X_3 = 1.6 μm.

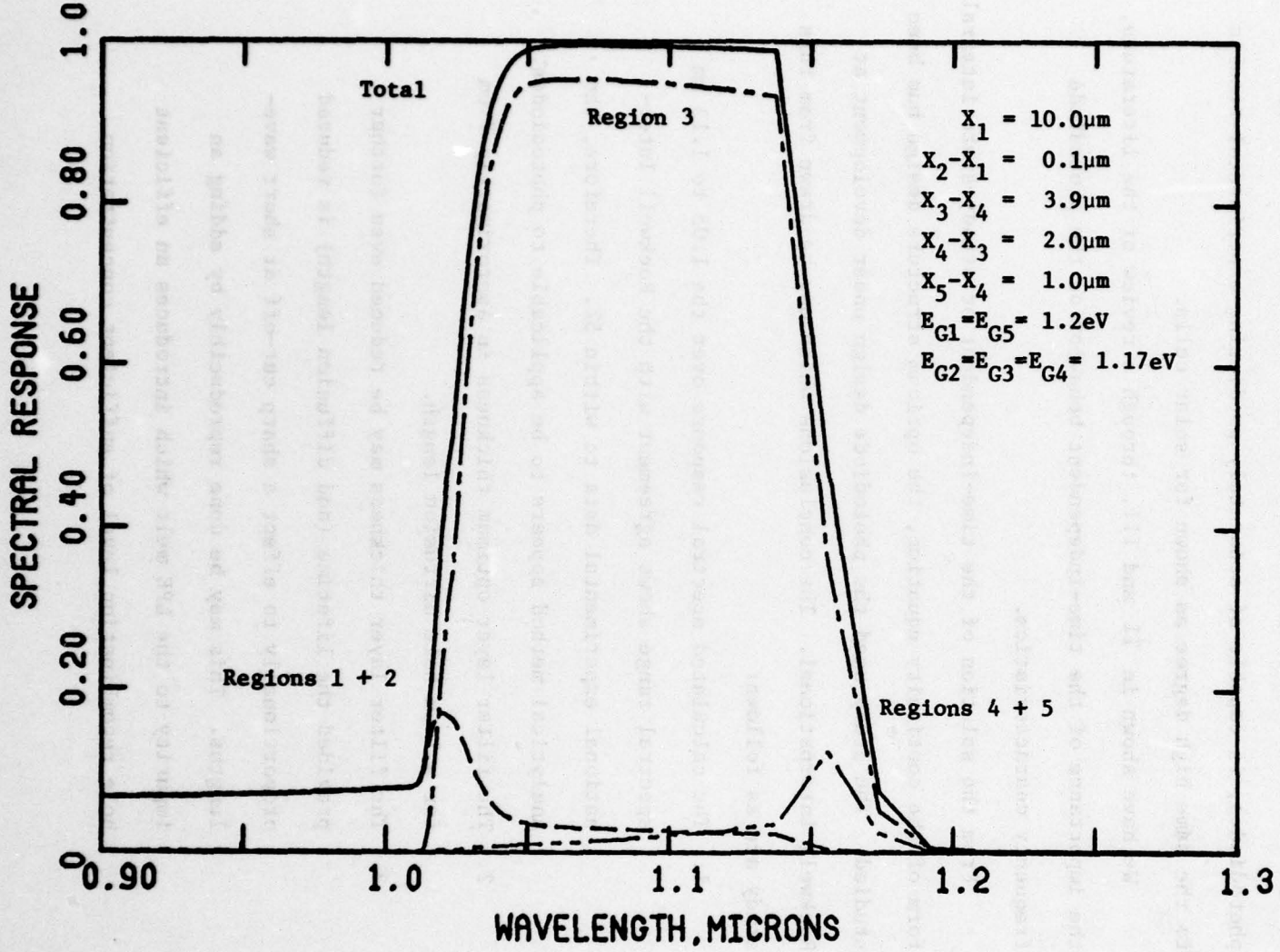

Figure 9(f). Photodiode spectral response in non-avalanche mode for X_4-X_3 = 2.0 μm.

SECTION VI

CONCLUDING SUMMARY

The purpose of this study was to demonstrate that the device analytical method developed for multilayer solar cells, when applied to photodiodes, is capable of accurately predicting experimental results to the same high degree as shown for solar cells.

We have shown in II and III, through a review of the literature, the importance of the time-independent behavior on the photodiode frequency characteristics.

From the solution of the time-independent or steady-state integral form of the continuity equation, the optimum structure design has been studied. The study used the photodiode design under development at Rockwell International. The conclusions which may be drawn from this study are as follows:

1. The calculated spectral response over the 1.05 to 1.15 μm spectral range shows agreement with the Rockwell International experimental data to within 5%. Therefore, the analytical method appears to be applicable to photodiodes.
2. The filter layer optimum thickness is approximately 7 μm for a 1 μm hole diffusion length.
3. The filter layer thickness may be reduced even further provided the lifetime (and diffusion length) is reduced proportionally to effect a sharp cut-off at short wavelengths. This may be done reproducibly by adding an impurity to the LPE melt which introduces an efficient hole recombination level of sufficient concentration.

4. The optimum thickness of the intrinsic layer is approximately 3.5 μm.
5. The filter layer bandgap determines the short wavelength cut-off.
6. The Region 4 optimum thickness is in the neighborhood of 0.4 to 1.0 μm.
7. Spectral response is independent of reverse voltage over wide limits.

SECTION VII

RECOMMENDATIONS

1. A study should be made to further extend the analysis to include frequency effects which reliably predicts device performance in the nonavalanche and avalanche modes.
2. The extended analysis should make use of the integral form of the time-dependent continuity equation and include the displacement current in the transport equations.
3. To realize the full potential of APDs fabricated from III-V materials requires a design study to determine those structures and materials that are more likely to and those that are less likely to give rise to sufficient gain to overcome preamplifier noise.
4. The time-independent and time-dependent electron and hole hole avalanche multiplication gain should be included in the solutions.
5. An optimum structure design study should be conducted to maximize S/N and frequency response with respect to signal generated photocurrent, phase difference between received signal and photocurrent, and preamplifier load impedance.
6. An optimum structure design study should be conducted to maximize bandwidth-gain as a function of material and structure parameters as well as preamplifier load impedance.
7. Study all the III-V materials combinations that may be used in diode structures. Select from and arrange in order of importance those combinations that give adequate S/N and frequency response for Air Force applications. In addition,

describe those materials combinations and the reasons for which APD performance is not suitable for Air Force applications.

8. Include in the boundary condition at each heterojunction of the diode structure a recombination term to describe heterofacial recombination processes that may occur.

REFERENCES

1. Dr. George H. Heilmeier, Keynote Speaker, Air Force Materials Laboratory Award Luncheon, WPAFB, Ohio, June 29, 1977, "Materials Technology - Some Challenges and Opportunities."

2. Contract Report AFAL-TR-76-113, Rockwell International, Thousand Oaks, California 91360, "1.06 Micrometer APD/Low Noise Preamplifier." June 1976.

3. Contract Report AFAL-TR-76-121, Rockwell International, Thousand Oaks, California 91360, "1.06 Micron Photodectector Development." October 1976.

3a. Contract Report AFAL-TR-76-74, Rockwell International, Thousand Oaks, California 91360, "1.06 Micrometer Avalanche Photodiode Detector." April 1977.

4. F.S. Goucher, G.B. Pearson, M. Sparks, G.K. Teal, and W. Shockley, Phys. Rev. 81, 637, Feb. 15, 1951.

5. K.G. McKay and K.B. McAfee, Phys. Rev. 91, Sept. 1, 1953.

6. R.P. Rietz, Rev. Sci. Int. 33, 994, 1962.

7. W.W. Gartner, Phys. Rev. 116, 84-87, Oct. 1, 1959.

8. R.B. Emmons and G. Lucovsky, IEEE-ED13, 297-305, March 1966.

9. R.B. Emmons, J. Appl. Phys. 38, 3705-3714, Aug. 1967.

10. J.J. Chang, IEEE-ED14, 139-145, March 1967.

11. I.M. Naqvi, Solid-State Elect. 16, 19-28, 1973.

12. G.T. Wright, Solid-State Elect. 16, 903-12, 1973.

13. S.M. Sze, Physics of Semiconductor Devices, John Wiley & Sons, New York 1969.

14. R.B. Emmons and G. Lucovsky, Proc. IEEE 52, 865, 1964.

15. L.K. Anderson and B.J. McMurtry, Appl. Opt. 5, 1573, 1966.

16. G. Lucovsky and R.B. Emmons, Appl. Opt. 4, 697, 1965.

17. K.M. Johnson, ISSCC Digest of Technical Papers 7, 64, 1964; K.M. Johnson, IEEE Trans. E.D.-12, 55, 1965.

18. R.L. Batdorf, A.G. Chynoweth, G.C. Dacey, and P.W. Foy, J. Appl. Phys. 31, 1153, 1960.

19. A. Goetzberger, B. McDonald, R.H. Haitz, and R.M. Scarlett, J. Appl. Phys. 34, 1591, 1963.

20. P.G. McMullin, L.K. Anderson, L.A. D'Asaro and A. Goetzberger, PGED Solid-State Device Research Conference, Boulder, Colorado, July 1-3, 1964; L.K. Anderson, P.G. McMullin, L.A. D'Asaro and A. Goetzberger, Appl. Phys. Lett. 6, 62, 1965.

21. W.T. Lynch and H. Melchoir, PGED Internat. Electron Device Meeting, Washington, D.C., Oct. 20-22, 1965; H. Melchoir and W.T. Lynch, Trans. IEEE Electron Devices ED-13, 829, 1966.

22. C.A. Lee and R.L. Batdorf, PGED Solid-State Research Conference, Boulder, Colorado, July 1-3, 1964.

23. W.T. Read, Jr., BSTJ 37, 401, 1958.

24. G. Lucovsky and R.B. Emmons, ISSCC Digest of Technical Papers 8, 52, 1965.

25. W. Van Roosbroeck, BSTJ 29, 560, 1950.

26. A.S. Tager, Soviet Phys. - Solid State 6, 1919, 1965.

27. R.J. McIntyre, PGED Solid-State Device Research Conference, Princeton, N.J., June 21-23, 1965; R.J. McIntyre, IEEE Trans. Electron Devices ED-13, 164, 1966.

*U.S.Government Printing Office: 1978 — 757-080/580